Tetrahedron 65 (2009) 2579–2590

Contents lists available at ScienceDirect

Tetrahedron

journal homepage: www.elsevier.com/locate/tet

Benzylic Newman–Kwart rearrangement of *O*-azidobenzyl thiocarbamates triggered by phosphines: pseudopericyclic [1,3] shifts via uncoupled concerted mechanisms

Mateo Alajarin *, Marta Marin-Luna, Maria-Mar Ortin, Pilar Sanchez-Andrada *, Angel Vidal *

Departamento de Química Orgánica, Facultad de Química, Universidad de Murcia, Campus de Espinardo, 30100 Murcia, Spain

ARTICLE INFO

Article history:
Received 28 November 2008
Received in revised form 29 December 2008
Accepted 5 January 2009
Available online 20 January 2009

Dedicated to Professor Josep Font on the occasion of his 70th birthday

Keywords:
Thiocarboxylates
Thione–thiol rearrangement
Pseudosigmatropic shift
Iminophosphoranes

ABSTRACT

A series of *O*-(*o*- and *p*-azido)benzyl thiocarbamates smoothly rearranged in the course of Staudinger imination reactions with tertiary phosphines, giving rise to the respective *S*-(*o*- and *p*-phosphinimino)benzyl thiocarbamates as a result of an oxygen to sulfur migration of the functionalized benzyl group. By contrary, their *m*-azido isomers did not rearrange under similar conditions. Computational investigations using DFT methods revealed the uncoupled concerted mechanisms of these 1,3-benzyl shifts via polar transition states with pseudopericyclic orbital topologies, with the benzyl group migrating in the plane of the thiocarbamate fragment.

1. Introduction

The Newman–Kwart rearrangement (NKR), reported for the first time in the sixties,[1] is a first-order unimolecular rearrangement converting *O*-aryl thiocarbamates into their *S*-aryl isomers under heating at 200–300 °C (Scheme 1). It is considered as a general and efficient method for converting phenols into thiophenols.[1c]

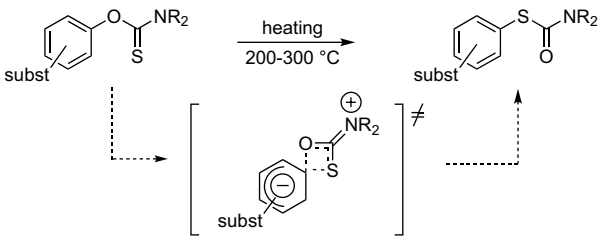

Scheme 1. Mechanism of the Newman–Kwart rearrangement.

This rearrangement is proposed to proceed via a zwitterionic four-center transition state, in accordance with the observation of the activating role played by electron-withdrawing substituents at the aromatic nucleus. Kinetic and linear free energy relationships are also in agreement with this mechanistic model.[2] The NKR is thermodynamically driven by the change from a weak C=S to a strong C=O double bond. Recent interest in the NKR focused on using microwaves as a mean for facilitating the conversion of electronically and sterically disfavored substituents.[3] As far as the benzylic variant of the NKR is concerned, the main theme of this article, it has been only briefly mentioned that *O*-benzyl *N*-phenylthiocarbamate rearranged smoothly to the *S*-benzyl analog under photochemical activation, in the context of a study on the rearrangement of a series of *O*-allylic partners.[4]

Whereas a variety of 1,3-allyl shifts between two heteroatoms, via [3,3] sigmatropic rearrangements are now well established,[5] similar 1,3-benzylic migrations have been scarcely reported. The oxygen to oxygen degenerate rearrangement of *O*-benzyl carboxylic esters is known to occur slowly at 260 °C with an activation energy over 190 kJ mol^{-1}.[6] The nitrogen to sulfur rearrangement of *N*-benzylpyridin-2-thiones producing 2-benzylthiopyridines also requires harsh thermal conditions.[7] The thermal *O*- to *S*-rearrangement of *O*-benzyl xanthate, a particular

* Corresponding authors. Tel.: +34 968 367497; fax: +34 968 364149 (M.A.); tel.: +34 968 367418; fax: +34 968 364149 (A.V.); tel.: +34 968 367425; fax: +34 968 364149 (P.S.A.).
E-mail addresses: alajarin@um.es (M. Alajarin), andrada@um.es (P. Sanchez-Andrada), vidal@um.es (A. Vidal).

0040-4020/$ – see front matter © 2009 Elsevier Ltd. All rights reserved.
doi:10.1016/j.tet.2009.01.064

case of the Schönberg rearrangement,[8] occurs at 150 °C yielding a complex mixture of products in which the expected $PhCH_2SC(O)SCH_3$ is the major component.[9] Similar thermal rearrangements occur at lower temperatures (100 °C) when catalyzed by tricaprylmethylammonium chloride[10] or pyridine-*N*-oxides.[11] The doubly benzylic *O*-benzhydryl xanthate was reported to rearrange at room temperature.[12]

Within the frame of our recent investigations on radical reactions of ketenimines,[13] we discovered an unexpected [1,3] shift of an *o*-functionalized benzylic fragment. When several *O*-benzyl thionoderivatives bearing an azide function at *ortho* position of the aromatic nucleus were submitted to the Staudinger imination reaction[14] of triphenylphosphine, the reaction products resulted to be the respective iminophosphoranes in which the benzylic fragment moved from O to S (Scheme 2).[13b]

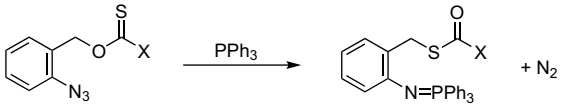

X = SCH_3
X = NHPh
X = OPh

Scheme 2. Benzylic O to S rearrangements.

These transformations captured our attention due to the smooth reaction conditions (Et_2O, 25 °C) under which they occur and their high reaction rates (less than 1 h for completion). Here we comment on the results obtained from a detailed study of this peculiar rearrangement. Such study has been carried out with a series of *O*-(azido)benzyl thiocarbamates in which the position of the azide function at the benzene ring varied from *ortho* to *meta* and *para*. The experimental data collected from the reaction of these species with tertiary phosphines, along with the conclusions drawn from an ad-hoc computational study, allow us to offer a rational explanation for the mechanistic course of such rearrangement, which accounts for the observed differences in reactivity between the diverse azido-substituted thiocarbamates.

2. Results and discussion

2.1. Experimental study

The treatment of *o*-azidobenzyl alcohols **1** with sodium hydride and arylisothiocyanates, in tetrahydrofuran solution at room temperature, cleanly provided the *N*-aryl-*O*-(*o*-azidobenzyl)thiocarbamates **2**. The Staudinger reaction of azides **2a–c** with tertiary phosphines, such as triphenylphosphine and tris(4-methylphenyl)phosphine, in diethyl ether solution at room temperature afforded the rearranged iminophosphoranes **3** in which the benzyl fragment is now linked to the S atom of the thiocarbamate function (Scheme 3, Table 1). The treatment of *O*-(2-azido-5-chlorobenzyl)thiocarbamates **2d**,**e** (R^1=Cl) with triphenylphosphine resulted in the formation of mixtures of the *S*-benzyl rearranged iminophosphoranes **3d**,**e** and its structural isomers, non-rearranged *O*-benzyl partners **4d**,**e**. Thus, the presence of a strong electron-withdrawing substituent, such as a chlorine atom in relative *para* position to the iminophosphorane group slightly decreases the rate of the [1,3] oxygen to sulfur migration. Subsequent heating of the mixtures (**3d**,**e**+**4d**,**e**) at 40 °C in the absence of solvent completed the conversion of **4d**,**e** into **3d**,**e** (Scheme 3).

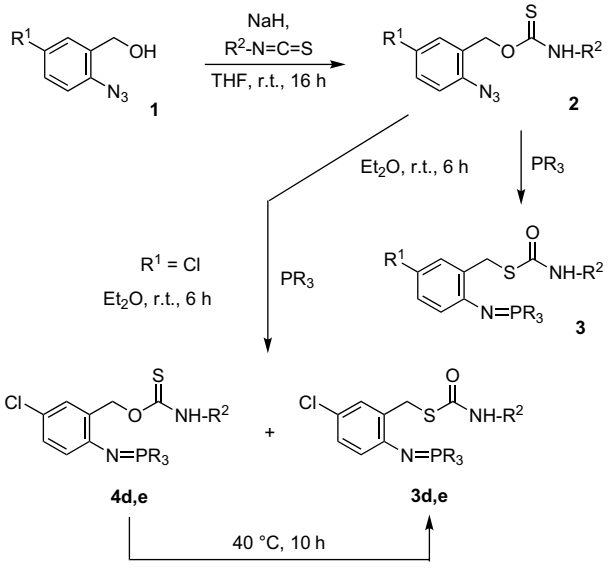

Scheme 3. Staudinger imination of *O*-(*o*-azidobenzyl) thiocarbamates **2**.

The determination of the structure of compounds **3** was essentially based on their ^{1}H and ^{13}C NMR spectroscopic data. Of particular relevance are the chemical shifts of the benzylic methylene protons in their ^{1}H NMR spectra, and the chemical shifts of the carbon atom of that group in their ^{13}C NMR spectra. In all cases, a notable upfield shift was observed for the above-mentioned nuclei when compared with the chemical shifts of the same nuclei in the corresponding azides **2**. Whereas the benzylic methylene protons appear at δ=5.43–5.48 ppm in the azides **2** the same protons in the iminophosphoranes **3** resonate at δ=4.36–4.54 ppm. The ^{13}C NMR spectra of azides **2** show the signals due to the benzylic carbon atom at δ=65.4–66.8 ppm, and those of iminophosphoranes **3** at δ=32.4–32.9 ppm. Also, in the ^{13}C NMR spectra of the iminophosphoranes **3** the signals that appear at higher δ values (δ=166.8–167.8 ppm) have undergone an upfield shift with respect to the same signals in the spectra of the azides **2** (δ=187.0–187.6 ppm), accounting for the presence of a carbonyl instead of a thiocarbonyl group in compounds **3**.

Next, we prepared the *O*-(*m*-azidobenzyl)thiocarbamates **6** by reaction of *m*-azidobenzyl alcohol **5** with sodium hydride and arylisothiocyanates. The treatment at room temperature of diethyl ether solutions of azides **6** with triphenylphosphine gave the iminophosporanes **7** (Scheme 4, Table 1), in which the benzyl group remains linked to the oxygen atom.

Table 1
Phosphazenes **3**, **7**, and **10**

Compound	R^1	R^2	R^3	R	Yield (%)
3a	H	4-Cl–C_6H_4		C_6H_5	40
3b	H	4-CH_3–C_6H_4		C_6H_5	66
3c	CH_3	C_6H_5		C_6H_5	87
3d	Cl	C_6H_5		C_6H_5	82
3e	Cl	4-CH_3–C_6H_4		C_6H_5	49
3f	H	4-CH_3–C_6H_4		4-CH_3–C_6H_4	80
7a		C_6H_5		C_6H_5	72
7b		4-CH_3–C_6H_4		C_6H_5	55
10a		CH_3–CH_2	H	C_6H_5	43
10b		C_6H_5–CH_2	H	C_6H_5	91
10c		C_6H_5	H	C_6H_5	92
10d		4-CH_3–C_6H_4	H	C_6H_5	54
10e		C_6H_5–CH_2	CH_3	C_6H_5	84
10f		C_6H_5–CH_2	H	$N(CH_3)_2$	64

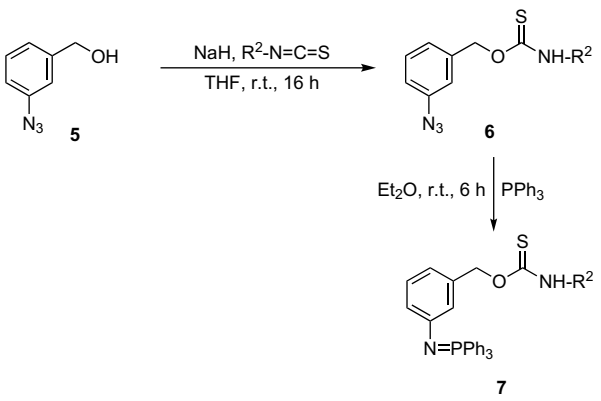

Scheme 4. Staudinger imination of *O*-(*m*-azidobenzyl) thiocarbamates **6**.

In the ^{1}H NMR spectra of compounds **7** the benzylic protons appear at δ=5.31–5.41 ppm. Their ^{13}C NMR spectra show the signals due to the benzylic carbon atom at δ=73.9–74.0 ppm, and that of the C=S group at δ=188.7–188.8 ppm.

As azidothiocarbamates **2** and **6** did not rearrange when kept in $CDCl_3$ solution for weeks, and given that the azide-lacking thiocarbamate 4-CH_3–$C_6H_4CH_2OC(S)NHPh$ remained intact when treated with PPh_3 (1 equiv) in diethyl ether,[15] it was clear that the rearrangement of *O*-(*o*-azidobenzyl)thiocarbamates **2** into **3** when converting the N_3 group into R_3P=N should be attributed to the intervention of the iminophosphorane function. Moreover, the absence of rearrangement in the transformation of the *meta* analogs **6**→**7** proved that such intervention is feasible when the R_3P=N is placed at *ortho* position but not at *meta*. In order to elucidate if this *ortho* activation is either due to some kind of intramolecular catalysis by virtue of the proximity between the iminophosphorane and thiocarbamate functions, or electronic in nature via resonance effects, we obviously assayed the Staudinger imination of phosphines with the *p*-azido-substituted thiocarbamates **9**.

O-(*p*-Azidobenzyl)thiocarbamates **9**, prepared from benzylic alcohols **8** by the standard methodology, reacted with triphenylphosphine to yield the rearranged *S*-[*p*-(phosphinimino)-benzyl]thiocarbamates **10** (Scheme 5, Table 1).

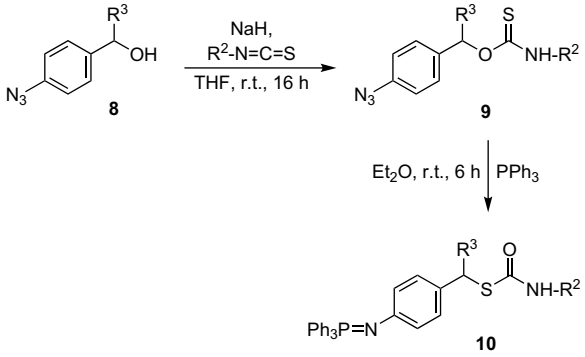

Scheme 5. Staudinger imination of *O*-(*p*-azidobenzyl) thiocarbamates **9**.

Compounds **10** were characterized by their analytical and spectral data, which were essentially similar to those of the analogous iminophosphoranes **3** (^{1}H NMR: benzylic CH_2 δ=3.90–4.10 ppm; ^{13}C NMR: benzylic CH_2 δ=33.9–34.6 ppm).

The benzylic rearrangement occurring in the transformation of **9** into **10** demonstrated that the mesomeric effect of the electron-donating [R_3P=N–↔R_3P^+–N^-–] group should be responsible for the rate increase allowing the occurrence of the 1,3-benzylic shift in the *ortho* and *para*-substituted thiocarbamates under very mild reaction conditions, in contrast with the lack of rearrangement in the *meta* isomers under similar conditions.

The activating effect of the electron-releasing R_3P=N substituents via resonance effects can be rationalized by assuming that the present *O*- to *S*-benzyl shift is basically cationotropic, its rate-determining step involving the heterolytic cleavage of the original C–O bond in a sense such that a cationic benzyl group is moving from the oxygen atom to the more nucleophilic sulfur of an anionic thiocarbamate fragment (Scheme 6).

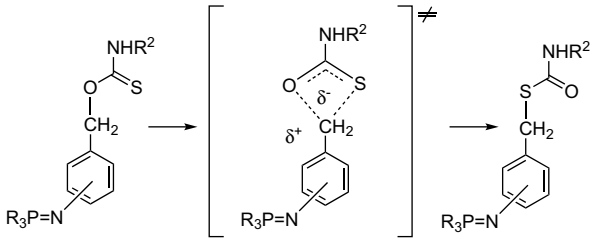

Scheme 6. Postulated mechanism for the 1,3-benzyl shift from O to S.

In contrast with the classic NKR of aryl groups, activated by electron-withdrawing substituents at the aromatic nucleus, the present benzylic version shows an inverse electronic situation as a result of the methylene group inserted between the oxygen and sulfur atoms. The activating effect of the *ortho* and *para*-R_3P=N electron-releasing substituents is reminiscent of the similar role played by *o*- and *p*-amino groups in 1,4- and 1,6-elimination reactions across benzylic fragments, which are on the basis of the very efficient use of aminobenzyloxycarbonyl self-elimination linkers for drug delivery applications, first introduced by Katzenellenbogen[16] and now widely used.[17] An example is represented in Scheme 7. With the amino group acylated the benzyloxycarbonyl linkers are stable under physiologic conditions, whereas deacylation to the free amino group promoted a rapid 1,6-elimination following which the formed cationic iminoquinone methide (in other words, an stabilized benzyl cation) is trapped by nucleophiles, e.g., H_2O, and the unstable carbamic or carbonic acid undergoes decarboxylation to release the active amine or alcohol drug. The triggering amino group has been also originated from inactive azido groups by chemical reduction[18] and quite recently by a Staudinger reaction with concurrent hydrolysis.[19]

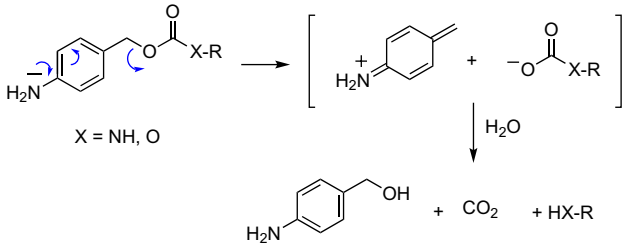

Scheme 7. Representative 1,6-elimination of unstable carbamic and carbonic acids.

In our hands, attempts to trap the putative migrating 'benzyl cation' in the O to S rearrangements **2**,**9**→**3**,**10** by externally added nucleophiles (H_2O, alcohols, amines) finished without success, thus pointing to the concerted nature of the rearrangement, as represented in Scheme 6. Most probably, there is not a real dissociation of the substrates into an ion pair, but a rapid [1,3] shift via a transition state, which should be zwitterionic in some extent, thus accounting for the observed rate acceleration by electronic effects.

A cross-over experiment was designed to distinguish if the title 1,3-benzyl migration is occurring via an intramolecular or intermolecular pathway. Thus we treated a 1:1 mixture of two

different *O*-(*o*-azidobenzyl)thiocarbamates, **2b** and **2c**, with triphenylphosphine under the standard conditions, affording a 1:1 mixture of the iminophosphoranes **3b** and **3c** in quantitative conversion (Scheme 8). No cross-over products could be detected in the ^{1}H NMR spectrum of the crude reaction mixture. The result of this experiment supports the intramolecularity of the rearrangements.

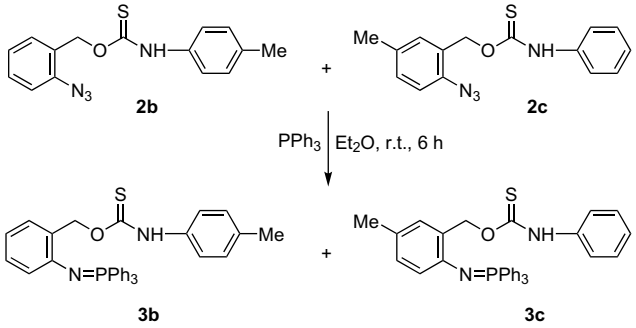

Scheme 8. Cross-over experiment of the benzylic NKR.

Phosphazides $R_3P{=}N{-}N{=}N{-}R'$ are known unstable intermediates in the Staudinger reaction. Nevertheless, some phosphazides, with the appropriate steric bulkiness and electronic properties of the substituents in the starting azide and phosphine, resist the thermal denitrogenation and are stable compounds at room temperature.[20] Particularly, the reaction of azides with electron-donating tris(dialkylamino)phosphines usually allows the isolation of stable phosphazides.

We carried out the reaction of azide **9b** (R^2=Ph-CH_2; R^3=H) with tris(dimethylamino)phosphine, with the aim of investigating the feasibility of the [1,3] *O*- to *S*-benzylic rearrangement in the resulting phosphazide. Thus, mixing azide **9b** and tris(dimethylamino)phosphine in diethyl ether at room temperature provided phosphazide **11**, in which the benzyl fragment has not experienced oxygen to sulfur migration (Scheme 9). When heated at 80 °C for 16 h in toluene solution compound **11** was transformed into the rearranged iminophosphorane **10f**.

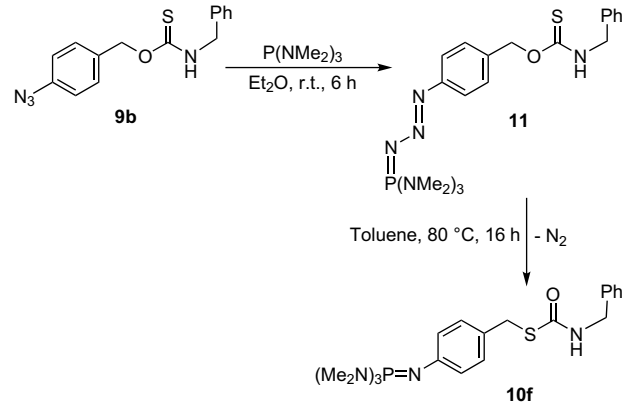

Scheme 9. Phosphazide isolation.

This result indicates that the *O*- to *S*-benzyl migration in the rearrangements discussed above seems to occur once the iminophosphorane function formed, and not at the stage of the intermediate phosphazides. It is reasonable that phosphazides are not better electron donors than iminophosphoranes, due to its extended conjugation. Whereas the instability in solution of phosphazides seems to have precluded detailed studies of their electronic effects as substituents on aromatic nuclei, it has been demonstrated that the most common iminophosphorane fragment, $Ph_3P{=}N$, served as an electron-donating substituent on a phenyl ring, slightly poorer than a Me_2N group when both are placed in *para* position (σ°=−0.40 vs −0.44).[21]

2.2. Computational study

To gain insight into the mechanism of the formation of *S*-benzylthiocarbamates from the corresponding *O*-benzylthiocarbamates presented in the experimental part of this work we have explored the potential energy surface associated to the rearrangement of the structurally simpler *O*-benzylthioesters **12a–c** leading to the *S*-benzylthioesters **13a–c** at the B3LYP/6-31+G** level of theory (Scheme 10). Additionally, the thiocarbamate **12d** was also investigated. These transformations were selected in order to compare the simplest unsubstituted case **12a** with one containing an electron-releasing NH_2 group (as representative of the experimentally used $N{=}PR_3$ functions) at a resonance active *para* (**12b**) or inactive *meta* (**12c**) position, as well with the simplest thiocarbamate **12d**.

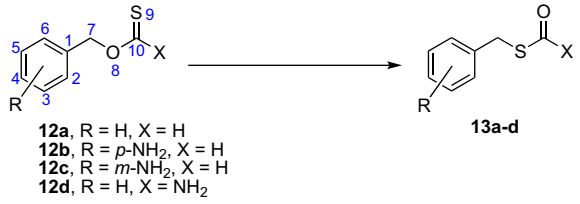

Scheme 10. 1,3-Benzyl shifts analyzed in the computational study.

We have successfully located the transition states **TSa–d** corresponding to the concerted, intramolecular [1,3]-benzyl shifts of the *O*-benzylthiocarboxylates **12** for converting into the corresponding *S*-benzyl isomers **13**. Figure 1 shows the geometries of **TSa–d**, including significant bond distances, and Figure 2 the optimized geometry of **TSa** showing the planes containing the interacting fragments. In Figure 3 a plot of the molecular electrostatic potential of **TSb** is shown. Figure 4 displays two qualitative reaction profiles at the B3LYP/6-31+G** theoretical level and the location of the stationary points for the 1,3-benzyl shift in the *O*-benzylthioester **12b**. In Tables 2 and 3 several relevant geometric and electronic parameters of the transition structures **TSa–d** are collected. Table 4 includes pertinent properties of ρ(r) computed at the relevant BCPs of the transition states **TSa–d**, whereas Table 5 contains the energy barriers for the transformations **12a–d**→**13a–d** computed at the B3LYP/6-31+G** and PCM–B3LYP/6-31+G** theoretical levels.

Transition structures **TSa–d** show interesting features that we will comment next. The benzylic carbon atom is almost planar, the sum of $C_1{-}C_7{-}H_{12}$, $C_1{-}C_7{-}H_{13}$, and $H_{12}{-}C_7{-}H_{13}$ angles range from 353° to 359°, the highest value is found in **TSb** (see Table 2). Thus, the hydrogen atoms attached to the benzylic carbon are placed almost in the mean plane that includes the phenyl ring and the benzylic carbon atom, denoted in Figure 2 as σ_1, which in turn forms an angle with the plane containing the thiocarboxylate moiety (σ_2) close to 100° (see Fig. 2). More importantly, the benzylic carbon atom is also found approximately in the plane defined by the thiocarboxylate fragment (σ_2). Consequently, the developing p orbital at the benzylic carbon is nearly perpendicular to the π-system of the O–C=S fragment. This geometry suggests that the main interactions between the benzylic and O–C=S fragments are those involving the lone pairs at the oxygen and sulfur heteroatoms with the p orbital at the benzylic carbon atom, which are nearly coplanar. This hypothesis has been

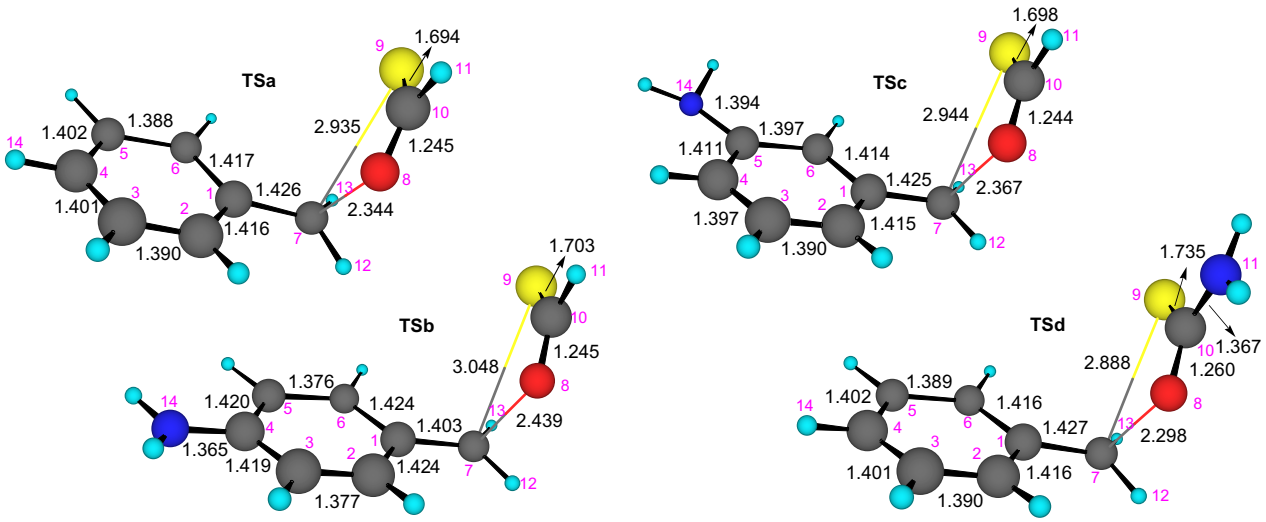

Figure 1. B3LYP/6-31+G** optimized geometries, showing relevant bond distances, of the transition structures **TSa–d** located for the [1,3]-benzyl shift transforming *O*-benzyl derivatives **12a–d** into their *S*-benzyl isomers **13a–d**.

confirmed by the results of the second-order perturbation theory analysis, which shows strong interactions from the donor lone pair orbitals at the oxygen and sulfur atoms with the transient p orbital at the benzylic carbon atom (see Supporting Information). Also it is worth to note that the sulfur and the oxygen atoms interact with the benzylic carbon on the same face of σ_1, and therefore we are dealing with a [1,3] shift where the benzyl group acts as the suprafacial component.

Among all the located transition states, **TSb** shows the longest C_7–O and C_7–S bonds as well as the shortest C_1–C_7 bond length (see Table 2). This latter finding indicates the effective delocalization of the lone pair at the N_{14} atom of the *para*-amino group into the benzylic fragment, and it is in agreement with the calculated $\sum\Delta_{N14}$ value, which is higher in **TSb** than in **TSc** (see Table 2), thus showing that the amino group in **TSb** is almost flat. Note that when the NH_2 group is placed in *meta* (**TSc**) the C_1–C_7 bond distance is similar to that found in **TSa** and **TSd**.

Bond index analysis can afford a deeper insight into the course of the chemical reactions than the simple study of the geometrical characteristics of the transition states. As demonstrated by Moyano et al.,[23] if the evolution of the bond indices corresponding to the bonds being made or broken in a chemical reaction is analyzed along the reaction path, a very precise image of the timing and the extent of the bond-breaking and the bond-forming processes at every point can be achieved. In order to perform the bond index analysis is convenient to define a relative variation of the bond index at the transition states, δB_i, for every bond, *i*, involved in the chemical reaction as:

$$\delta B_i = \frac{B_i^{TS} - B_i^{R}}{B_i^{P} - B_i^{R}},$$

where the superscripts TS, R, and P refer to the TS, reactant, and product, respectively. It is also possible to calculate the percentage of evolution[24] of the bond order of each one along the rearrangement by using the following expression:

$$\%E_v = \delta B_i \times 100.$$

Besides, the average value, δB_{av}, calculated as:

$$\delta B_{av} = \frac{1}{n}\sum_{i=1}^{n} \delta B_i,$$

where *n* is the number of bonds directly involved in the reaction, affords a measure of the degree of advancement of a TS along the reaction path. One can also obtain information of the absolute asynchronicity, *A*, of a chemical reaction, using the expression developed by Moyano et al.[23]

Thus, to follow the nature of these [1,3] shifts, we have computed the Wiberg bond indices by using the Natural Bond Orbital analysis at the σC_7–O_8 and πC_{10}–S_9 bonds, which are breaking, and at the σC_7–S_9 and πC_{10}–O_8 bonds, which are forming along the chemical reaction. These values are summarized in Table 3. The C_7–O_8 bond-breaking process is the most advanced motion among all the bond-breaking/making processes ($\%E_v$=75–81%), showing that this bond is almost broken at the TS. **TSb** displays the highest calculated value (81%). By contrast, the C_7–S_9 bond formation process is the reaction coordinate that shows less progress for all these shifts, displaying a small evolution percentage (23–31%, the lowest value shown by **TSb**). Accordingly, by considering the high degree of evolution found for the C_7–O_8

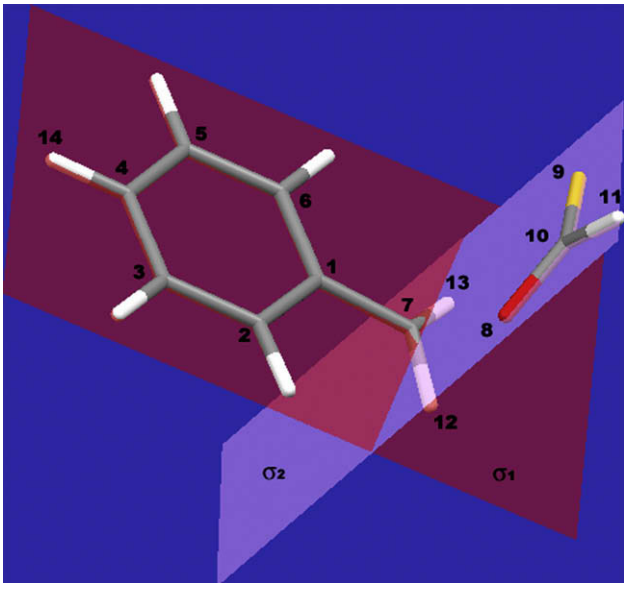

Figure 2. B3LYP/6-31+G** optimized geometry of transition structure **TSa** showing the planes containing the interacting benzylic and O–C=S fragments.[22]

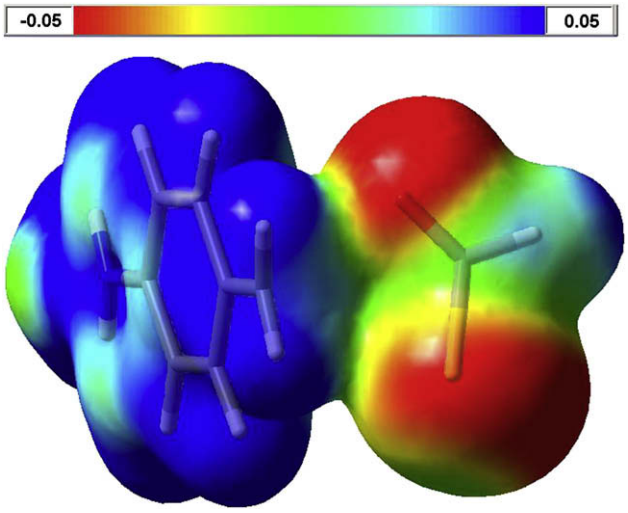

Figure 3. MESP of **TSb** plotted onto the electron density surface with an isovalue of 0.01 a.u. showing the highly polar character of the system. The color coding is shown at the top.

breaking bond and the little evolution found for the C_7–S_9 forming bond, the migration of the benzyl fragment from the oxygen to the sulfur atom can be classified as a concerted asynchronic process, accounting for the development of electron charge separation between the benzyl and O–C═S fragments at these transition states (see below). The O_8–C_{10} and S_9–C_{10} bonds, that evolve from single to double bond and from double to single bond, respectively, are almost simultaneous processes, although the evolution is higher for the O_8–C_{10} (63–66%) than for the S_9–C_{10} bond (57–58%). Thus, the elongation of the C_7–O_8 bond and, in lower extension, the O_8–C_{10} double bond formation can be seen as the driving forces of these rearrangements.

The δB_{av} values summarized in Table 3 show that transition structures **TSa–d** have somewhat more product-like character than reactant-like one, being the C_7–S_9 bond formation, as inferred from the $\%E_v$ values, the only motion in which these TSs have a reactant-like character.

An analysis of the NBO charges proves the zwitterionic character of these transition states, more notorious in **TSb**. Thus, the migrating benzyl group carries a positive charge ranging from +0.47 to +0.58 (see $\sum q_b$ in Table 3). The sum of natural charges at the O–C═S moiety is obviously of opposite sign. Therefore, this analysis

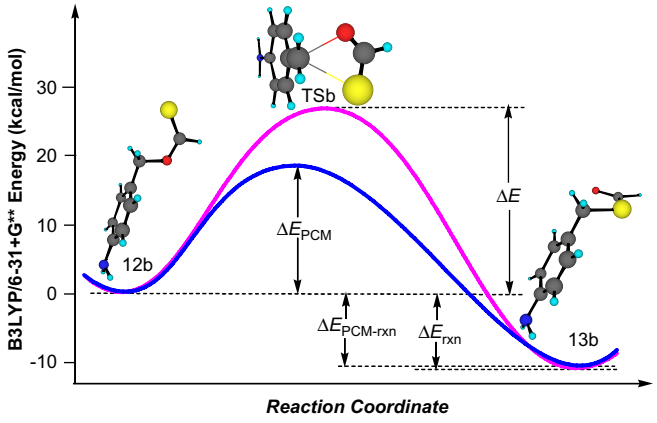

Figure 4. Qualitative reaction profiles at the B3LYP/6-31+G** and PCM–B3LYP/6-31+G** theoretical levels and the location of the stationary points for the 1,3-benzyl shift **12b**→**13b**.

Table 2
Angle between the σ_1 and σ_2 planes[a] ($\Lambda\sigma_1$–σ_2), sum of angles at C_7 ($\sum\Lambda_{C7}$) and N_{14} ($\sum\Lambda_{N14}$), and bond distances for the C_7–O, C_7–S, and C_1–C_7 bonds computed for the transition structures **TSa–d** at the B3LYP/6-31+G** theoretical level

	$\Lambda\sigma_1$–σ_2[b]	$\sum\Lambda_{C7}$[b]	$\sum\Lambda_{N14}$[b]	δ[c] (C_7–O)	δ[c] (C_7–S)	δ[c] (C_1–C_7)
TSa	103.8	353.4		2.33	2.93	1.43
TSb	101.2	358.6	358.1	2.44	3.05	1.40
TSc	103.3	356.7	345.1	2.37	2.94	1.42
TSd	102.9	356.2		2.30	2.89	1.43

[a] See Figures 1 and 2 for notation.
[b] In degrees.
[c] In Angstroms.

suggests a noteworthy assistance of Coulomb interaction between both charged fragments stabilizing the TS. The charge separation can also be visualized by computing the molecular electrostatic potential (MESP) values. In Figure 3 the MESP values for **TSb**, reflecting the electron-rich and electron-deficient regions of the molecule, are shown.

Note that **TSb** is the structure among the four transition states that shows the highest value of the dipolar moment, the highest value of $\%E_v$ of the C_7–O_8 bond-breaking process and the lowest of the C_7–S_9 bond formation ones, the highest value of charge separation between the O–C═S and benzyl fragments, the highest asynchronicity value, and also the most favorable transition state (see below in Table 5).

The contribution of the NH_2 group at the *para* position of the phenyl ring for stabilizing the positive charge at the benzylic carbon atom of **TSb** is apparent by comparing the sum of natural charges at the benzylic fragment ($\sum q_b$) with the natural charge calculated at the benzyl carbon atom (q_{C7}). Thus, in spite of the highest value of $\sum q_b$ shown by **TSb** ($\sum q_b$=+0.58), the lowest positive charge at that carbon is also found in **TSb** (q_{C7}=+0.33).

According to all these data, an important bond deficiency exists in the transition states, i.e., the bond-breaking C_7–O_8 process is more advanced that the C_7–S_9 bond-forming one, and this is translated into the important polar character reflected in the sum of natural charges at the interacting fragments. In the four transition states **TSa–d** the electronic deficiency created at the benzylic carbon atom by the breaking of the C_7–O_8 bond is compensated by formation of a partial π bond with the adjacent carbon atom at the phenyl ring (C_1) rather than by the incipient formation of the σC_7–S_9 bond. The contraction of the C_1–C_7 bond in going either from reactants or from products to the transition states supports this hypothesis. Thus, the bond indices corresponding to the C_1–C_7 bonds in **TSa–d** range from 1.26 to 1.37, the highest value shown by **TSb**, whereas a notorious decrease of these values can be observed in reactants and products (see Table 3). Once again, the contribution of the NH_2 group at the *para* position of the phenyl ring for stabilizing the positive charge at the benzylic carbon atom of **TSb** is evident.

With the aim to gain further insight into the nature of these 1,3-benzyl shifts we have used the AIM[25] methodology to calculate several properties of the electron density at pertinent bond critical points (BCPs) of the TSs (Table 4).

The sign of the Laplacian of the electron density, $\nabla^2[\rho(r)]$, at a BCP is determined by which energy is in excess over the viral 2:1 average of kinetics to potential energy. A negative value of $\nabla^2[\rho(r)]$ is related with the excess of the potential energy at the BCP, which means that the electronic charge is concentrated in the inter-nuclear region and therefore shared by two nuclei, as occurs in shared electron (covalent) interactions. By contrary, positive values of $\nabla^2[\rho(r)]$ at a BCP reveal an excess in kinetic energy and indicates depletion of electronic charge along the bond path, as is the case of closed shell interactions (ionic

Table 3
Natural charges at the benzylic carbon atom (q_{C7}), sums of natural charges at the benzyl fragment ($\sum q_b$), dipolar moments (μ), degrees of advancement of the TSs (δB_{av}), asynchronicity values (A), Wiberg bond indices (B_i), and percentages of evolution through the chemical process of the bond indexes computed for the transition structures **TSa–d** at the B3LYP/6-31+G** theoretical level

	q_{C7}[a,b]	$\sum q_b$[b]	μ[c]		C_7–O_8	C_7–S_9	O_8–C_{10}	S_9–C_{10}	C_1–C_7
TSa	0.34	0.47	5.11	B_i^R	0.830	0.019	1.127	1.798	1.024
				B_i^{TS}	0.215	0.317	1.533	1.443	1.267
				B_i^P	0.008	0.977	1.764	1.171	1.030
				$\%E_v$	74.8	31.1	63.7	56.7	
						δB_{av}=0.57; A=0.15			
TSb	0.33	0.58	9.68	B_i^R	0.819	0.018	1.136	1.789	1.033
				B_i^{TS}	0.164	0.239	1.548	1.432	1.364
				B_i^P	0.008	0.969	1.759	1.177	1.036
				$\%E_v$	80.8	23.2	66.1	58.3	
						δB_{av}=0.57; A=0.20			
TSc	0.35	0.49	5.48	B_i^R	0.829	0.019	1.131	1.793	1.023
				B_i^{TS}	0.204	0.313	1.544	1.433	1.271
				B_i^P	0.008	0.977	1.758	1.177	1.029
				$\%E_v$	76.1	30.1	65.9	58.4	
						δB_{av}=0.58; A=0.16			
TSd	0.39	0.52	4.07	B_i^R	0.836	0.015	1.046	1.580	1.020
				B_i^{TS}	0.213	0.309	1.427	1.258	1.258
				B_i^P	0.007	0.982	1.650	1.027	1.029
				$\%E_v$	75.1	30.4	63.1	58.2	
						δB_{av}=0.57; A=0.15			

[a] Natural charge with hydrogens summed into the carbon atom.
[b] In atomic units.
[c] In Debyes.

bonds). For the transition states **TSa–d** the computed values for $\nabla^2[\rho(r)]$ at the C_7–O_8 and C_7–S_9 BCPs are positive, ranging from +0.083 to +0.104 and from +0.048 to +0.057 a.u., respectively, indicating very little sharing between the corresponding two atomic basins. Additionally, the electronic density energy, $H(r)$ [$H(r)=G(r)+V(r)$] evaluated at a BCP can be used to compare the kinetics $G(r)$ and potential $V(r)$ energy densities on an equal footing. For all interactions with significant sharing of electrons $H(r)$ is negative reflecting the covalent character of the interaction. In the cases of the BCPs at C_7–O_8 and C_7–S_9 the kinetic energy density dominates over the potential energy density and $H(r)$ is therefore positive, as anticipated for closed shell interactions. These results reveal the ionic character of the C_7–O_8 and C_7–S_9 breaking/forming bonds at the transition structures **TSa–d**, and are in agreement with the assistance of Coulomb interaction stabilizing the TSs proposed above.

The calculated energy barriers for these [1,3] shifts are collected in Table 5. All conversions resulted to be exothermic by 10–11 kcal mol^{-1}. The barrier for the conversion **12b**→**13b** is calculated to be the lowest (the qualitative reaction profile is represented in Fig. 4), the barrier computed for the transformations **12a**→**13a** and **12c**→**13c** is comparable, and the highest energy barrier is shown by the conversion **12d**→**13d**. The latter result can be explained by the presence of the amino group attached to the carbon atom of the thiocarbamate function, which is expected to destabilize the polar transition structure **TSd** due to the electron-releasing character of the amino group. On the contrary, the amino group at the *para* position in **12b** accounts for the stabilization of the transition state **TSb** due to its ability to share the partial positive charge at the benzylic carbon atom. Obviously, this is not possible when the amino group is not present or placed in the *meta* position (**TSa** and **TSc**).

To evaluate the solvent influence in these processes we have optimized all the stationary points considering the solvent effect of diethyl ether (ε=4.335) by the PCM method. The results are included in Table 5. With the inclusion of diethyl ether the transition states are stabilized relative to reactants, whereas reactants and products are similarly stabilized. Thus, whereas the exothermicities do not vary significantly, the energy barriers decrease around 3 kcal mol^{-1} in all the cases except for the conversion **12b**→**13b**, where the lowering of the energy barrier is calculated to be of 8.6 kcal mol^{-1} (see Table 5). This result is in accordance with the higher dipolar moment of **TSb** when compared with the rest of the transition structures (see Table 3).

Table 4
Relevant properties of $\rho(r)$ computed at the BCPs for the breaking C_7–O_8 and the forming C_7–S_9 in the transition states **TSa–d** at the B3LYP/6-31+G** level of theory[a]

BCP		TSa	TSb	TSc	TSd
C_7–O_8	$\rho(r)$	0.0353	0.0292	0.0336	0.0376
	$\nabla^2[\rho(r)]$	0.0941	0.0831	0.0911	0.1036
	$G(r)$	0.0231	0.0197	0.0221	0.0257
	$H(r)$	0.0004	0.0011	0.0007	0.0002
C_7–S_9	$\rho(r)$	0.0205	0.0171	0.0203	0.0222
	$\nabla^2[\rho(r)]$	0.0501	0.0478	0.0503	0.0565
	$G(r)$	0.0107	0.0097	0.0107	0.0122
	$H(r)$	0.0018	0.0023	0.0019	0.0019

[a] $\rho(r)$ is the electron density (e/au^3); $\nabla^2[\rho(r)]$ is the Laplacian (e/au^5); $G(r)$ is the kinetic energy density, and $H(r)$ is the energy density.

Table 5
Energy barriers (kcal mol^{-1}) computed for the transformations **12a–d** into **13a–d** through the transition states **TSa–d**[a] at the B3LYP31+G** and PCM–B3LYP/6-31+G** theoretical levels

	B3LYP[b]		PCM–B3LYP[c]	
	ΔE	ΔE_{rxn}	ΔE_{PCM}	$\Delta E_{PCM\text{-}rxn}$
12a→**13a** (R=H, X=H)	32.41	−11.09	29.19	−11.12
12b→**13b** (R=*p*-NH_2, X=H)	26.69	−10.58	18.09	−10.51
12c→**13c** (R=*m*-NH_2, X=H)	32.07	−11.27	28.54	−11.14
12d→**13d** (R=H, X=NH_2)	35.97	−11.70	33.03	−11.38

[a] See Figure 4 for the notation of the energy barriers.
[b] Energies computed on the fully optimized B3LYP/6-31+G** geometries. The ZPVE corrections, which were not scaled, were computed at the same level and have been included.
[c] Energies computed on the fully optimized PCM–B3LYP/6-31+G** geometries using diethyl ether as solvent. The ZPVE corrections, which were not scaled, were computed at the same level and have been included.

2.3. Summary and conclusions

In summary, this theoretical study predicts that the 1,3-benzyl shift in *O*-benzylthioesters leading to *S*-benzylthioesters takes place by a concerted mechanism involving polar transition structures where the planes containing the benzylic and the thiocarboxylate interacting fragments form an angle close to 100°. The examination of its geometry along with the NBO analysis unveil that the main interactions involve the lone pairs at the sulfur and oxygen atoms with the transient p orbital at the benzylic carbon atom, pointing to a transition state of pseudopericyclic topology. That is, the interacting orbitals are not in a closed loop as expected for a pericyclic transition state (see below).

The cleavage of the bond between the oxygen atom and the benzylic carbon and the formation of the bond between the sulfur atom and the same carbon atom take place very asynchronously. The first occurs in going from the reactant to the transition state, where that bond is almost broken, whereas the formation of the latter occurs on going downhill from the TS to the product. There is a substantial charge separation between the benzylic and thiocarboxylate fragments involving a noteworthy Coulomb interaction assistance stabilizing the TSs. The substitution at the *para* position of the phenyl ring by electron-releasing substituents (an amino group in the conversion **12b**→**13b**) results in a substantial lowering of the energy barrier for the 1,3-benzyl shift by stabilizing the positive charge at the benzylic carbon atom, the asynchronicity of the reaction being simultaneously enhanced.

It is worth to remark that we are dealing with a strongly asynchronous rearrangement, of the type Jenks qualified as 'uncoupled concerted',[26] with a TS where the C–O bond breaking is much more advanced than the C–S bond formation. In such uncoupled concerted process there is no reaction intermediate (i.e., an ion pair in the present case) but there is no coupling between bond formation and bond cleavage, both occurring in the same kinetic step but not simultaneously. This particular mechanism, at the concerted/stepwise boundary, has been also termed as a 'two-phase process' by other authors.[27]

In the course of our computational study all attempts to locate a transition structure for the formation of an intermediate ion pair failed, the saddle-point searches invariably converging on the concerted transition states. Such concerted TSs and the hypothetical transition structures for ion pair formation would involve nearly complete breaking of the C–O bonds and the difference between the two types of saddle points is that the concerted TSs also involve C–S formation in some extent. However, as we have stated above, the degree to which C–S bonds have progressed in the located TSs is very minor. As a result, such structures are very close to those expected for the transition states forming ion pairs. Rather than involving two separate transition structures with extremely similar geometries it seems that the stepwise and concerted pathways have merged in the located TSs corresponding to the uncoupled concerted one.

As far as the activating role of electron-donor substituents (*o*- and *p*-$R_3P{=}N$ in the experimental work, *o*- and *p*-NH_2 in the calculations) is concerned, it is important to note that stepwise and uncoupled concerted processes should show similar structure–reactivity relationships, because the unsymmetrical transition state of the uncoupled concerted one closely resembles one or the other transition structure of the stepwise reaction. Moreover, the build up of positive charge at the benzylic carbon atom, especially in **TSb**, has been clearly shown by the calculations.

On the basis of the orbital topologies of the transition states, these O to S rearrangements here discussed can be qualified as *pseudosigmatropic* shifts of benzyl groups by virtue of their pseudopericyclic characteristics. Pseudopericyclic reactions are a subset of pericyclic reactions, which contain one or more orbital disconnections in the cyclic array of overlapping orbitals.[28,29] The orbital topologies of the present rearrangements are not those expected for classic pericyclic 1,3-benzyl shifts as the breaking and forming sigma bonds do not overlap with the π system of the thiocarboxylate fragment, but instead they are nearly orthogonal. It is worth to emphasize that the first pseudosigmatropic shift of a methylene group has been very recently reported by de Lera and co-workers.[30]

A notorious consequence of the geometric characteristics of these transition states is that chiral benzyl fragments should retain the absolute configuration of its benzylic carbon atom at the end of the rearrangement (note that the sulfur and oxygen atoms interact with the benzylic carbon atom by the same face of the plane containing the benzyl fragment, and therefore, in a classical pericyclic [1,3] shift the benzyl fragment would be labeled as the suprafacial component, thus resulting in the retention of its configuration). We believe that many other heteroatom to heteroatom 1,3-benzyl shifts can also involve pseudopericyclic transition states and occur with retention of configuration. This latter proposal has been recently demonstrated by the elegant experiments carried out by Tsuji and Richard with an enantiomerically enriched phenylethyl thiobenzoate.[31]

3. Experimental

3.1. General

All melting points are uncorrected. Infrared (IR) spectra were recorded as Nujol emulsions. ^{1}H NMR spectra were recorded in $CDCl_3$ at 300 or 400 MHz. ^{13}C NMR spectra were recorded in $CDCl_3$ at 75 or 100 MHz. The chemical shifts are expressed in parts per million, relative to Me_4Si at δ=0.00 ppm for ^{1}H, while the chemical shifts for ^{13}C are reported relative to the resonance of $CDCl_3$ δ=77.10 ppm or DMSO-d_6 δ=35.35 ppm.

2-Azidobenzyl alcohol **1a**,[32] 2-azido-5-methylbenzyl alcohol **1b**,[33] 2-azido-5-chlorobenzyl alcohol **1c**,[34] 3-azidobenzyl alcohol **5**,[35] and 4-azidobenzyl alcohol **8a**[18b] were prepared following literature procedures.

3.2. General procedure for the preparation of 4-azido-α-methylbenzyl alcohol 8b ($R^3=CH_3$)

To a solution of 4-amino-α-methylbenzyl alcohol (1.18 g, 7.25 mmol) in a mixture of water (30 mL) and concentrated sulfuric acid (5 mL), cooled at −5 °C, was added dropwise a solution of sodium nitrite (0.86 g, 12.5 mmol) in 10 mL of water. After 30 min of stirring, a solution of sodium azide (0.81 g, 12.5 mmol) in 10 mL of water was added dropwise, and stirring was continued for 16 h. The mixture was extracted with dichloromethane (2×30 mL). The combined organic layers were washed with water (2×100 mL) and dried over anhydrous magnesium sulfate. The solvent was removed under reduced pressure and the resulting oil was purified by column chromatography [silica gel, hexanes/diethyl ether (1:4, v/v)].

Yield 70%; oil; IR (Neat) 3363, 2099, 1606, 1582, 1507, 1449, 1418, 1294, 1204, 1180, 1129, 1088, 1009, 898, 834 cm^{-1}; ^{1}H NMR (DMSO-d_6, 400 MHz) δ 1.29 (d, 3H, *J*=6.4 Hz), 4.70 (qd, 1H, *J*=6.4, 4.4 Hz), 5.20 (d, 1H, *J*=4.4 Hz), 7.04 (d, 2H, *J*=8.4 Hz), 7.36 (d, 2H, *J*=8.4 Hz); ^{13}C NMR (DMSO-d_6, 100 MHz) δ 25.9, 67.5, 118.7, 126.9, 137.4 (s), 144.5 (s); HRMS (EI): *m*/*z*: calcd for $C_8H_9N_3O$: 163.0746; found: 163.0750.

3.3. General procedure for the preparation of the *O*-(azidobenzyl)thiocarbamates 2, 6, and 9

To a solution of the azidobenzyl alcohol **1**, **5** or **8** (5 mmol) and the isothiocyanate (5 mmol) in anhydrous tetrahydrofuran (25 mL)

was added sodium hydride (60% in oil; 0.25 g, 6.25 mmol). The reaction mixture was stirred at room temperature in an atmosphere of nitrogen for 16 h. Then the tetrahydrofuran was removed under reduced pressure and the resulting material was partitioned between dichloromethane (30 mL) and water (30 mL). The organic layer was separated and dried over anhydrous magnesium sulfate. After evaporation of the solvent the residue was purified by silica gel column chromatography using hexanes/diethyl ether (7:3, v/v) as eluent.

3.4. Characterization data for products 2, 6, and 9

3.4.1. O-(2-Azidobenzyl)-N-(4-chlorophenyl)thiocarbamate ***2a***

Yield 51%; mp 120–122 °C (colorless prisms); IR (Nujol) 3245, 2130, 2120, 1599, 1551, 1492, 1406, 1345, 1301, 1218, 1091, 1021, 824, 753 cm^{-1}; ^1H NMR (DMSO-d_6, 60 °C, 300 MHz) δ 5.48 (s, 2H), 7.21 (td, 1H, J=7.5, 1.2 Hz), 7.31–7.37 (m, 3H), 7.43–7.55 (m, 4H); ^{13}C NMR (DMSO-d_6, 60 °C, 75 MHz) δ 66.8, 118.4, 123.6, 124.6, 126.3 (s), 128.1, 128.6 (s), 129.8, 130.0, 136.8 (s), 137.8 (s), 187.0 (s); HRMS (EI): m/z: calcd for $C_{14}H_{11}ClN_2OS$: 290.0281; found: 290.0283.

3.4.2. O-(2-Azidobenzyl)-N-(4-methylphenyl)thiocarbamate ***2b***

Yield 71%; mp 104–106 °C (colorless prisms); IR (Nujol) 3213, 2126, 1591, 1541, 1489, 1405, 1360, 1309, 1286, 1182, 1155, 1097, 1120, 834, 751 cm^{-1}; ^1H NMR (DMSO-d_6, 60 °C, 300 MHz) δ 2.26 (s, 3H), 5.47 (s, 2H), 7.11 (d, 2H, J=8.4 Hz), 7.20 (t, 1H, J=7.3 Hz), 7.31–7.47 (m, 5H), 10.90 (s, 1H); ^{13}C NMR (DMSO-d_6, 60 °C, 75 MHz) δ 19.6, 66.4, 118.2, 122.1, 124.4, 126.6 (s), 128.2, 129.3, 129.5, 133.7 (s), 135.2 (s), 137.5 (s), 187.1 (s); HRMS (EI): m/z: calcd for $C_{15}H_{14}N_2OS$: 270.0827; found: 270.0828.

3.4.3. O-(2-Azido-5-methylbenzyl)-N-phenylthiocarbamate ***2c***

Yield 54%; mp 128–130 °C (colorless prisms); IR (Nujol) 3229, 2128, 2087, 1592, 1552, 1494, 1405, 1344, 1288, 1201, 1186, 1079, 1058, 799, 750 cm^{-1}; ^1H NMR (DMSO-d_6, 60 °C, 400 MHz) δ 2.28 (s, 3H), 5.43 (s, 2H), 7.13 (t, 1H, J=7.2 Hz), 7.21 (d, 1H, J=8.0 Hz), 7.25–7.33 (m, 4H), 7.51 (br s, 2H), 11.01 (s, 1H); ^{13}C NMR (DMSO-d_6, 60 °C, 100 MHz) δ 19.9, 66.7, 118.3, 122.2, 124.6, 126.1, 128.1, 130.1, 130.5, 134.1 (s), 134.9 (s), 137.8 (s), 187.0 (s); HRMS (EI): m/z: calcd for $C_{15}H_{14}N_2OS$: 270.0827; found: 270.0830.

3.4.4. O-(2-Azido-5-chlorobenzyl)-N-phenylthiocarbamate ***2d***

Yield 74%; mp 125–130 °C (colorless prisms); IR (Nujol) 3199, 3045, 2125, 1560, 1449, 1402, 1291, 1220, 1203, 1184, 1057, 888, 805, 741, 687 cm^{-1}; ^1H NMR (DMSO-d_6, 60 °C, 300 MHz) δ 5.45 (s, 2H), 7.15 (t, 1H, J=8.4 Hz), 7.30–7.36 (m, 3H), 7.45–7.50 (m, 4H), 11.04 (s, 1H); ^{13}C NMR (DMSO-d_6, 60 °C, 75 MHz) δ 66.6, 121.0, 123.0, 125.4, 128.8, 129.2 (s), 129.4 (s), 129.7, 129.8, 137.2 (s), 138.6 (s), 187.6 (s); HRMS (EI): m/z: calcd for $C_{14}H_{11}ClN_2OS$: 290.0281; found: 290.0284.

3.4.5. O-(2-Azido-5-chlorobenzyl)-N-(4-methylphenyl)-thiocarbamate ***2e***

Yield 46%; mp 145–147 °C (colorless prisms); IR (Nujol) 3202, 2125, 2087, 1533, 1396, 1336, 1305, 1185, 1169, 1112, 1038, 866, 812, 720 cm^{-1}; ^1H NMR (DMSO-d_6, 60 °C, 300 MHz) δ 3.10 (s, 3H), 5.43 (s, 2H), 7.12 (d, 2H, J=8.1 Hz), 7.34–7.48 (m, 5H), 10.95 (s, 1H); ^{13}C NMR (DMSO-d_6, 60 °C, 75 MHz) δ 20.7, 65.4, 121.0, 123.0, 129.3, 129.4 (s), 129.6, 129.8, 134.8 (s), 136.0 (s), 137.2 (s), 187.4 (s); HRMS (EI): m/z: calcd for $C_{15}H_{13}ClN_2OS$: 304.0437; found: 304.0430.

3.4.6. O-(3-Azidobenzyl)-N-phenylthiocarbamate ***6a***

Yield 89%; mp 112–114 °C (colorless prisms); IR (Nujol) 3229, 3167, 2121, 1598, 1587, 1556, 1406, 1343, 1294, 1206, 1191, 1044, 865, 782, 752, 683 cm^{-1}; ^1H NMR (DMSO-d_6, 60 °C, 300 MHz) δ 5.57 (s, 2H), 7.06–7.17 (m, 3H), 7.24 (d, 1H, J=7.5 Hz), 7.32 (t, 2H, J=7.5 Hz), 7.42 (t, 1H, J=7.8 Hz), 7.50 (br s, 2H), 11.02 (s, 1H); ^{13}C NMR (DMSO-d_6, 60 °C, 75 MHz) δ 69.9, 118.0, 118.4, 122.3, 124.2, 124.6, 128.2, 129.7, 137.8 (s), 139.3 (s), 187.1 (s); HRMS (EI): m/z: calcd for $C_{14}H_{12}N_2OS$: 256.0670; found: 256.0670.

3.4.7. O-(3-Azidobenzyl)-N-(4-methylphenyl)thiocarbamate ***6b***

Yield 54%; mp 94–97 °C (colorless prisms); IR (Nujol) 3230, 3170, 2111, 1597, 1587, 1551, 1406, 1292, 1223, 1191, 1056, 810, 780, 737, 681 cm^{-1}; ^1H NMR (DMSO-d_6, 60 °C, 400 MHz) δ 2.26 (s, 3H), 5.55 (s, 2H), 7.06 (d, 1H, J=6.4 Hz), 7.11–7.16 (m, 3H), 7.22–7.24 (d, 1H, J=7.2 Hz), 7.32–7.45 (m, 3H), 10.96 (s, 1H); ^{13}C NMR (DMSO-d_6, 60 °C, 100 MHz) δ 20.0, 69.8, 118.0, 118.4, 122.3, 124.2, 128.6, 129.7, 134.0 (s), 137.9 (s), 139.3 (s), 187.0 (s); HRMS (EI): m/z: calcd for $C_{15}H_{14}N_2OS$: 270.0827; found: 270.0827.

3.4.8. O-(4-Azidobenzyl)-N-ethylthiocarbamate ***9a***

The ^1H and ^{13}C NMR spectra of compound **9a** at room temperature (in $CDCl_3$) displayed doubling of the majority of signals, suggesting the presence of two rotamers in a ratio 1:1.7.

Yield 41%; mp 72–75 °C (colorless prisms); IR (Nujol) 3128, 3071, 2111, 2064, 1597, 1445, 1334, 1307, 1285, 1217, 1202, 1140, 1062, 1012, 828, 809, 720 cm^{-1}; ^1H NMR ($CDCl_3$, 300 MHz) δ 1.07 (t, $3H_{minor}$, J=7.5 Hz), 1.15 (t, $3H_{mayor}$, J=7.5 Hz), 3.20–3.29 (m, $2H_{minor}$), 3.47–3.56 (m, $2H_{mayor}$), 5.36 (s, $2H_{mayor}$), 5.43 (s, $2H_{minor}$), 6.25 (br s, $1H_{mayor}$), 6.73 (br s, $1H_{minor}$), 6.92–6.97 (m, 4H), 7.28–7.33 (m, 4H); ^{13}C NMR ($CDCl_3$, 75 MHz) δ 13.7, 14.2, 38.2, 40.2, 70.8, 72.4, 119.0, 119.1, 129.8, 129.9, 132.2 (s), 132.5 (s), 140.0 (s), 140.1 (s), 189.4 (s), 189.5 (s); HRMS (EI): m/z: calcd for $C_{10}H_{12}N_2OS$: 208.0670; found: 208.0672.

3.4.9. O-(4-Azidobenzyl)-N-benzylthiocarbamate ***9b***

The ^1H and ^{13}C NMR spectra of compound **9b** at room temperature (in $CDCl_3$) displayed doubling of the majority of signals, suggesting the presence of two rotamers in a ratio 1:2.

Yield 73%; mp 90–91 °C (colorless prisms); IR (Nujol) 3222, 2114, 1548, 1507, 1400, 1341, 1285, 1243, 1217, 1201, 1177, 1083, 1061, 960, 816, 738 cm^{-1}; ^1H NMR ($CDCl_3$, 400 MHz) δ 4.35 (d, 2H, J=5.6 Hz), 4.67 (d, 2H, J=5.6 Hz), 5.39 (s, 2H), 5.43 (s, 2H), 6.48 (s, 1H), 6.90 (s, 1H), 6.92–7.31 (m, 18H); ^{13}C NMR ($CDCl_3$, 100 MHz) δ 47.3, 49.4, 71.3, 72.6, 119.0, 127.5, 127.8, 127.9, 128.7, 129.9, 130.0, 132.0 (s), 132.4 (s), 136.3 (s), 136.5 (s), 140.1 (s), 189.4 (s), 190.0 (s); HRMS (EI): m/z: calcd for $C_{15}H_{14}N_2OS$: 270.0827; found: 270.0827.

3.4.10. O-(4-Azidobenzyl)-N-phenylthiocarbamate ***9c***

Yield 78%; mp 114–115 °C (colorless prisms); IR (Nujol) 3238, 2120, 2081, 1597, 1547, 1510, 1494, 1446, 1408, 1336, 1307, 1292, 1212, 1172, 1136, 1015, 752, 686 cm^{-1}; ^1H NMR (DMSO-d_6, 300 MHz) δ 5.55 (s, 2H), 7.10–7.16 (m, 3H), 7.31 (t, 2H, J=7.8 Hz), 7.46–7.49 (m, 4H), 10.98 (s, 1H); ^{13}C NMR (DMSO-d_6, 75 MHz) δ 70.3, 118.8, 122.2, 124.5, 128.1, 129.5, 132.5 (s), 137.8 (s), 139.0 (s), 187.1 (s); HRMS (EI): m/z: calcd for $C_{14}H_{12}N_2OS$: 256.0670; found: 256.0672.

3.4.11. O-(4-Azidobenzyl)-N-(4-methylphenyl)thiocarbamate ***9d***

Yield 55%; mp 92–95 °C (colorless prisms); IR (Nujol) 3193, 2118, 1606, 1587, 1537, 1506, 1395, 1348, 1249, 1175, 1128, 1042, 834, 816, 783 cm^{-1}; ^1H NMR (DMSO-d_6, 300 MHz) δ 2.26 (s, 3H), 5.53 (s, 2H), 7.11 (d, 4H, J=7.5 Hz), 7.36 (br s, 2H), 7.46 (d, 2H, J=7.5 Hz), 10.91 (s, 1H); ^{13}C NMR (DMSO-d_6, 75 MHz) δ 20.0, 70.1, 118.8, 122.2, 128.6, 129.5, 132.5 (s), 133.9 (s), 135.3 (s), 139.0 (s), 187.0 (s); HRMS (EI): m/z: calcd for $C_{15}H_{14}N_2OS$: 270.0827; found: 270.0831.

3.4.12. O-(4-Azido-α-methylbenzyl)-N-benzylthiocarbamate ***9e***

The ^1H and ^{13}C NMR spectra of compound **9e** at room temperature (in $CDCl_3$) displayed doubling of the majority of signals, suggesting the presence of two rotamers in a ratio 1:1.7.

Yield 88%; oil; IR (Neat) 3267, 2104, 1659, 1606, 1508, 1454, 1394, 1342, 1294, 1174, 1129, 1057, 1029, 1001, 968, 895, 833, 698 cm^{-1}; ^1H NMR ($CDCl_3$, 400 MHz) δ 1.48 (d, $3H_{minor}$, J=6.8 Hz), 1.50 (d, $3H_{mayor}$, J=6.8 Hz), 4.35 (d, $2H_{minor}$, J=6.0 Hz), 4.56–4.68 (m, $2H_{mayor}$), 5.55 (br s, $1H_{minor}$), 6.37 (q, $1H_{minor}$, J=6.8 Hz), 6.41 (q, $1H_{mayor}$, J=6.8 Hz), 6.49 (br s, $1H_{mayor}$), 6.84–7.28 (m, 18H); ^{13}C NMR ($CDCl_3$, 100 MHz) δ 21.8, 21.9, 47.1, 49.2, 77.3, 79.1, 118.8, 118.9, 119.0, 127.4, 127.6, 127.7, 127.79, 127.82, 127.86, 127.89, 128.5, 128.6, 128.69, 128.7, 136.5 (s), 136.6 (s), 137.7 (s), 138.1 (s), 138.7 (s), 139.4 (s), 139.5 (s), 139.9 (s), 188.7 (s), 189.3 (s); HRMS (EI): m/z: calcd for $C_{16}H_{16}N_2OS$: 284.0983; found: 284.0989.

3.5. General procedure for the preparation of the phosphazenes 3, 7, and 10

To a solution of the corresponding azide **2**, **6** or **9** (5 mmol) in anhydrous diethyl ether (15 mL) the tertiary phosphine (5 mmol) was added. The resulting mixture was stirred at room temperature in an atmosphere of nitrogen for 3–6 h. Then the precipitated compounds were isolated by filtration.

3.6. Characterization data for products 3, 7, and 10

3.6.1. Phosphazene **3a** (R^1=H; R^2=4-Cl–C_6H_4; R=C_6H_5)

Yield 40%; mp 90–91 °C (colorless prisms); IR (Nujol) 3289, 1678, 1591, 1481, 1436, 1396, 1342, 1303, 1145, 1111, 1021, 826, 716, 693 cm^{-1}; ^1H NMR ($CDCl_3$, 400 MHz) δ 4.51 (s, 2H), 6.45 (d, 1H, J=7.6 Hz), 6.64 (t, 1H, J=7.6 Hz), 6.81 (td, 1H, J=7.6, 1.2 Hz), 7.16 (d, 2H, J=8.8 Hz), 7.25–7.27 (m, 2H), 7.33–7.35 (m, 1H), 7.42–7.46 (m, 6H), 7.51–7.55 (m, 3H), 7.70–7.75 (m, 6H), 7.78 (s, 1H); ^{13}C NMR ($CDCl_3$, 100 MHz) δ 32.9, 117.8, 121.1 (d, J=9.8 Hz), 121.5, 128.0, 128.7 (d, J=12.0 Hz), 128.9, 130.1 (d, J=2.1 Hz), 130.9 (d, J=99.1 Hz) (s), 131.7 (s), 131.9 (d, J=2.9 Hz), 132.6 (d, J=9.7 Hz), 136.8 (s), 149.3 (s), 167.8 (s); ^{31}P NMR ($CDCl_3$, 121.4 MHz, H_3PO_4) δ 3.83; HRMS (ESI): m/z: calcd for $C_{32}H_{26}ClN_2OPS$: 552.1192; found: 552.1204.

3.6.2. Phosphazene **3b** (R^1=H; R^2=4-CH_3–C_6H_4; R=C_6H_5)

Yield 66%; mp 118–121 °C (colorless prisms); IR (Nujol) 3266, 1674, 1643, 1592, 1517, 1481, 1309, 1239, 1152, 1109, 1049, 1021, 813, 750, 715, 694 cm^{-1}; ^1H NMR ($CDCl_3$, 400 MHz) δ 2.28 (s, 3H), 4.54 (s, 2H), 6.45 (d, 1H, J=7.6 Hz), 6.63 (t, 1H, J=7.2 Hz), 6.81 (td, 1H, J=7.6, 1.6 Hz), 7.04 (d, 2H, J=8.0 Hz), 7.22 (d, 2H, J=8.4 Hz), 7.36 (dt, 1H, J=5.2, 2.0 Hz), 7.42–7.47 (m, 6H), 7.50–7.55 (m, 3H), 7.73–7.79 (m, 6H), 7.80 (s, 1H); ^{13}C NMR ($CDCl_3$, 100 MHz) δ 20.8, 32.8, 117.4, 120.2, 120.7 (d, J=9.8 Hz), 127.8, 128.6 (d, J=10.0 Hz), 129.4, 129.9 (d, J=2.0 Hz), 131.1 (d, J=99.6 Hz) (s), 131.7 (d, J=2.3 Hz), 132.0 (d, J=11.9 Hz) (s), 132.5 (d, J=9.7 Hz), 133.6 (s), 135.6 (s), 149.5 (s), 167.4 (s); ^{31}P NMR ($CDCl_3$, 121.4 MHz, H_3PO_4) δ 2.76; HRMS (ESI): m/z: calcd for $C_{33}H_{29}N_2OPS$: 532.1738; found: 532.1752.

3.6.3. Phosphazene **3c** (R^1=CH_3; R^2=R=C_6H_5)

Yield 87%; mp 89–91 °C (colorless prisms); IR (Nujol) 3256, 3178, 1679, 1640, 1600, 1491, 1437, 1346, 1309, 1237, 1186, 1143, 1107, 1035, 1023, 811, 751, 721, 693 cm^{-1}; ^1H NMR ($CDCl_3$, 400 MHz) δ 2.19 (s, 3H), 4.51 (s, 2H), 6.37 (d, 1H, J=8.0 Hz), 6.63 (dd, 1H, J=8.0, 1.6 Hz), 7.04 (t, 1H, J=7.2 Hz), 7.19–7.26 (m, 3H), 7.34 (d, 2H, J=7.6 Hz), 7.42–7.46 (m, 6H), 7.50–7.54 (m, 3H), 7.65 (s, 1H), 7.72–7.77 (m, 6H); ^{13}C NMR ($CDCl_3$, 100 MHz) δ 20.4, 32.7, 120.1, 120.5 (d, J=9.6 Hz), 123.9, 126.5 (s), 128.4, 128.5 (d, J=11.9 Hz), 128.8, 130.5, 130.9 (d, J=95.6 Hz) (s), 131.6 (d, J=2.0 Hz), 132.5 (d, J=9.7 Hz), 138.1 (s), 146.6 (s), 167.5 (s); ^{31}P NMR ($CDCl_3$, 121.4 MHz, H_3PO_4) δ 2.77; HRMS (ESI): m/z: calcd for $C_{33}H_{29}N_2OPS$: 532.1738; found: 532.1743.

3.6.4. Phosphazene **3d** (R^1=Cl; R^2=R=C_6H_5)

Yield 82%; mp 78–80 °C (colorless prisms); IR (Nujol) 3162, 1592, 1546, 1437, 1282, 1185, 1170, 1109, 1022, 1004, 904, 753, 720, 690 cm^{-1}; ^1H NMR ($CDCl_3$, 400 MHz) δ 4.36 (s, 2H), 6.22 (d, 1H, J=8.4 Hz), 6.64 (dd, 1H, J=8.4, 2.8 Hz), 6.95 (t, 1H, J=7.6 Hz), 7.15 (t, 2H, J=7.6 Hz), 7.22–7.26 (m, 3H), 7.31 (s, 1H), 7.33–7.37 (m, 6H), 7.41–7.45 (m, 3H), 7.60–7.65 (m, 6H); ^{13}C NMR ($CDCl_3$, 100 MHz) δ 32.4, 119.8, 121.3 (d, J=9.9 Hz), 121.6 (s), 124.0, 127.4, 128.6 (d, J=12.0 Hz), 128.9, 129.5, 130.4 (d, J=100.0 Hz) (s), 131.8 (d, J=2.7 Hz), 132.4 (d, J=9.7 Hz), 133.4 (d, J=22.7 Hz) (s), 137.9 (s), 148.2 (s), 166.9 (s); ^{31}P NMR ($CDCl_3$, 121.4 MHz, H_3PO_4) δ 4.06; HRMS (ESI): m/z: calcd for $C_{32}H_{26}ClN_2OPS$: 552.1192; found: 552.1212.

3.6.5. Phosphazene **3e** (R^1=Cl; R^2=4-CH_3–C_6H_4; R=C_6H_5)

Yield 49%; mp 84–87 °C (colorless prisms); IR (Nujol) 3199, 3175, 1643, 1631, 1589, 1542, 1437, 1400, 1353, 1315, 1186, 1170, 1107, 1021, 812, 719, 694 cm^{-1}; ^1H NMR ($CDCl_3$, 300 MHz) δ 2.20 (s, 3H), 4.36 (s, 2H), 6.23 (d, 1H, J=8.4 Hz), 6.65 (dd, 1H, J=8.4, 2.7 Hz), 6.96 (d, 2H, J=8.4 Hz), 7.13–7.16 (m, 2H), 7.20 (s, 1H), 7.23 (t, 1H, J=2.7 Hz), 7.30–7.39 (m, 6H), 7.43–7.47 (m, 3H), 7.61–7.67 (m, 6H); ^{13}C NMR ($CDCl_3$, 75 MHz) δ 20.8, 32.4, 120.1, 121.4 (d, J=9.8 Hz), 121.8 (s), 127.4, 128.6 (d, J=12.0 Hz), 129.4, 129.5, 130.4 (d, J=100.6 Hz) (s), 131.9 (d, J=2.1 Hz), 132.4 (d, J=9.7 Hz), 133.4 (s), 133.7 (d, J=4.4 Hz) (s), 135.3 (s), 166.8 (s); ^{31}P NMR ($CDCl_3$, 121.4 MHz, H_3PO_4) δ 4.48; HRMS (ESI): m/z: calcd for $C_{33}H_{28}ClN_2OPS$: 566.1348; found: 566.1351.

3.6.6. Phosphazene **3f** (R^1=H; R^2=R=4-CH_3–C_6H_4)

Yield 80%; mp 118–121 °C (colorless prisms); IR (Nujol) 3128, 1584, 1537, 1510, 1483, 1405, 1358, 1332, 1204, 1184, 1106, 1019, 827, 808, 753, 662, 649 cm^{-1}; ^1H NMR ($CDCl_3$, 400 MHz) δ 2.17 (s, 3H), 2.28 (s, 9H), 4.42 (s, 2H), 6.35 (d, 1H, J=7.6 Hz), 6.51 (t, 1H, J=7.2 Hz), 6.70 (td, 2H, J=7.6, 2.0 Hz), 6.91 (d, 2H, J=8.0 Hz), 7.09–7.14 (m, 8H), 7.24 (dt, 1H, J=7.2, 2.4 Hz), 7.49–7.455 (m, 6H); ^{13}C NMR ($CDCl_3$, 100 MHz) δ 20.7, 21.5, 32.7, 117.2, 120.3, 120.8 (d, J=9.9 Hz), 127.4 (s), 127.6, 129.2 (d, J=12.3 Hz), 129.3, 129.8, 131.7 (s), 132.1 (s), 132.5 (d, J=101. Hz), 133.4 (s), 135.5 (s), 141.9 (s), 149.7 (s), 167.6 (s); ^{31}P NMR ($CDCl_3$, 121.4 MHz, H_3PO_4) δ 3.78; HRMS (ESI): m/z: calcd for $C_{36}H_{35}N_2OPS$: 574.2208; found: 574.2217.

3.6.7. Phosphazene **7a** (R^2=R=C_6H_5)

Yield 72%; mp 124–126 °C (colorless prisms); IR (Nujol) 3057, 1591, 1514, 1483, 1438, 1344, 1331, 1313, 1303, 1194, 1176, 1103, 1035, 1022, 921, 778, 712, 699 cm^{-1}; ^1H NMR ($CDCl_3$, 60 °C, 400 MHz) δ 5.31 (s, 2H), 6.58 (d, 1H, J=7.2 Hz), 6.65 (dd, 1H, J=8.0, 1.2 Hz), 6.77 (s, 1H), 6.89 (t, 1H, J=7.6 Hz), 7.01 (t, 1H, J=7.2 Hz), 7.14–7.18 (m, 2H), 7.23 (br s, 2H), 7.29–7.33 (m, 6H), 7.37–7.41 (m, 3H), 7.62–7.67 (m, 6H), 8.09 (s, 1H); ^{13}C NMR ($CDCl_3$, 60 °C, 100 MHz) δ 74.0, 117.3, 122.1, 123.4, 123.6, 125.3, 128.5 (d, J=11.8 Hz), 128.7, 128.9, 131.3 (d, J=99.2 Hz) (s), 131.6 (d, J=2.6 Hz), 132.6 (d, J=9.3 Hz), 135.5 (s), 137.6 (s), 151.5 (s), 188.7 (s); ^{31}P NMR ($CDCl_3$, 121.4 MHz, H_3PO_4) δ 3.82; HRMS (ESI): m/z: calcd for $C_{32}H_{27}N_2OPS$: 518.1582; found: 518.1592.

3.6.8. Phosphazene **7b** (R^2=4-CH_3–C_6H_4; R=C_6H_5)

Yield 55%; mp 144–146 °C (colorless prisms); IR (Nujol) 3055, 1594, 1522, 1483, 1437, 1334, 1317, 1304, 1264, 1196, 1178, 1106, 1036, 999, 836, 780, 744, 719, 694 cm^{-1}; ^1H NMR ($CDCl_3$, 60 °C, 400 MHz) δ 2.31 (s, 3H), 5.41 (s, 2H), 6.68 (d, 1H, J=7.2 Hz), 6.75 (d, 1H, J=7.6 Hz), 6.86 (s, 1H), 6.99 (t, 1H, J=8.0 Hz), 7.07–7.09 (m, 2H), 7.20 (br s, 2H), 7.40–7.44 (m, 6H), 7.48–7.52 (m, 3H), 7.73–7.78 (m, 6H), 8.05 (br s, 1H); ^{13}C NMR ($CDCl_3$, 60 °C, 100 MHz) δ 20.9, 73.9, 117.4, 122.4 (s), 123.5 (d, J=4.6 Hz), 123.6 (d, J=5.6 Hz), 128.6 (d, J=12.0 Hz), 128.8, 129.5, 131.5 (d, J=99.3 Hz) (s), 131.6 (d, J=2.8 Hz), 132.7 (d, J=9.5 Hz), 135.1 (s), 135.7 (s), 151.6 (d, J=2.0 Hz) (s), 188.8

(s); ^{31}P NMR ($CDCl_3$, 121.4 MHz, H_3PO_4) δ 2.26; HRMS (ESI): *m*/*z*: calcd for $C_{33}H_{29}N_2OPS$: 532.1738; found: 532.1748.

3.6.9. Phosphazene ***10a*** *(R^2=CH_3CH_2; R^3=H; R=C_6H_5)*

Yield 43%; mp 87–89 °C (colorless prisms); IR (Nujol) 3150, 1658, 1603, 1504, 1437, 1287, 1176, 1145, 1103, 995, 831, 805, 744, 717, 694 cm^{-1}; ^{1}H NMR ($CDCl_3$, 400 MHz) δ 1.01 (t, 3H, *J*=7.2 Hz), 3.18–3.21 (m, 2H), 3.96 (s, 2H), 5.27 (s, 1H), 6.63 (d, 2H, *J*=7.6 Hz), 6.87 (d, 2H, *J*=7.6 Hz), 7.32–7.36 (m, 6H), 7.40–7.44 (m, 3H), 7.62–7.67 (m, 6H); ^{13}C NMR ($CDCl_3$, 100 MHz) δ 14.5, 33.9, 35.9, 122.8 (d, *J*=17.8 Hz), 125.6 (s), 128.1 (d, *J*=11.9 Hz), 128.8, 130.5 (d, *J*=98.9 Hz) (s), 131.2 (d, *J*=2.7 Hz), 132.1 (d, *J*=9.4 Hz), 149.9 (s); ^{31}P NMR ($CDCl_3$, 121.4 MHz, H_3PO_4) δ 3.39; HRMS (ESI): *m*/*z*: calcd for $C_{28}H_{27}N_2OPS$: 470.1582; found: 470.1584.

3.6.10. Phosphazene ***10b*** *(R^2=C_6H_5–CH_2; R^3=H; R=C_6H_5)*

Yield 91%; mp 154–155 °C (colorless prisms); IR (Nujol) 3148, 1602, 1541, 1503, 1436, 1317, 1271, 1141, 1108, 1019, 960, 949, 939, 851, 719, 693 cm^{-1}; ^{1}H NMR ($CDCl_3$, 300 MHz) δ 4.02 (s, 2H), 4.38 (d, 2H, *J*=5.7 Hz), 5.50 (s, 1H), 6.64 (d, 2H, *J*=8.1 Hz), 6.90 (d, 2H, *J*=8.1 Hz), 7.16–7.25 (m, 5H), 7.33–7.46 (m, 9H), 7.63–7.69 (m, 6H); ^{13}C NMR ($CDCl_3$, 75 MHz) δ 34.4, 45.2, 123.2 (d, *J*=17.5 Hz), 125.9 (s), 127.5, 127.6, 128.5 (d, *J*=11.7 Hz), 129.2, 130.6 (d, *J*=106.9 Hz) (s), 131.7 (d, *J*=2.6 Hz), 132.5 (d, *J*=9.6 Hz), 137.7 (s), 150.1 (s), 167.6 (s); ^{31}P NMR ($CDCl_3$, 121.4 MHz, H_3PO_4) δ 4.10; HRMS (ESI): *m*/*z*: calcd for $C_{33}H_{29}N_2OPS$: 532.1738; found: 532.1739.

3.6.11. Phosphazene ***10c*** *(R^2=C_6H_5; R^3=H; R=C_6H_5)*

Yield 92%; mp 160–162 °C (colorless prisms); IR (Nujol) 3165, 1683, 1601, 1551, 1502, 1435, 1308, 1249, 1163, 1150, 1129, 1110, 1017, 999, 853, 720 cm^{-1}; ^{1}H NMR ($CDCl_3$, 400 MHz) δ 4.04 (s, 2H), 6.64 (d, 2H, *J*=8.0 Hz), 6.91 (d, 2H, *J*=8.0 Hz), 6.98–7.02 (m, 2H), 7.19–7.23 (m, 2H), 7.29–7.32 (m, 2H), 7.33–7.38 (m, 6H), 7.41–7.46 (m, 3H), 7.63–7.68 (m, 6H); ^{13}C NMR ($CDCl_3$, 100 MHz) δ 34.3, 119.3, 122.9 (d, *J*=17.8 Hz), 123.8 (s), 125.0 (s), 128.1 (d, *J*=12.0 Hz), 128.6, 128.9, 130.4 (d, *J*=99.3 Hz) (s), 131.3 (d, *J*=2.5 Hz), 132.1 (d, *J*=9.6 Hz), 137.4 (s), 150.1 (s); ^{31}P NMR ($CDCl_3$, 121.4 MHz, H_3PO_4) δ 3.57; HRMS (ESI): *m*/*z*: calcd for $C_{32}H_{27}N_2OPS$: 518.1582; found: 518.1587.

3.6.12. Phosphazene ***10d*** *(R^2=4-CH_3–C_6H_4; R^3=H; R=C_6H_5)*

Yield 54%; mp 139–143 °C (colorless prisms); IR (Nujol) 3154, 1685, 1603, 1541, 1503, 1435, 1306, 1238, 1150, 1108, 819, 719, 692 cm^{-1}; ^{1}H NMR ($CDCl_3$, 400 MHz) δ 2.29 (s, 3H), 4.10 (s, 2H), 6.73 (d, 2H, *J*=8.0 Hz), 6.98 (d, 2H, *J*=8.0 Hz), 7.07 (d, 2H, *J*=8.0 Hz), 7.24–7.26 (m, 3H), 7.40–7.44 (m, 6H), 7.48–7.52 (m, 3H), 7.71–7.76 (m, 6H); ^{13}C NMR ($CDCl_3$, 100 MHz) δ 20.8, 34.6, 119.9, 123.3 (d, *J*=17.8 Hz), 125.7 (s), 128.6 (d, *J*=11.9 Hz), 129.3, 129.5, 130.8 (d, *J*=98.9 Hz) (s), 131.7 (d, *J*=2.6 Hz), 132.6 (d, *J*=9.7 Hz), 134.0 (s), 135.3 (s), 150.4 (s); ^{31}P NMR ($CDCl_3$, 121.4 MHz, H_3PO_4) δ 3.83; HRMS (ESI): *m*/*z*: calcd for $C_{33}H_{29}N_2OPS$: 532.1738; found: 532.1746.

3.6.13. Phosphazene ***10e*** *(R^2=C_6H_5–CH_2; R^3=CH_3; R=C_6H_5)*

Yield 84%; mp 155–157 °C (colorless prisms); IR (Nujol) 3166, 1656, 1603, 1534, 1506, 1432, 1366, 1325, 1222, 1177, 1106, 1027, 998, 828, 718, 691 cm^{-1}; ^{1}H NMR ($CDCl_3$, 400 MHz) δ 1.66 (d, 3H, *J*=7.2 Hz), 4.43 (d, 2H, *J*=5.6 Hz), 4.68 (q, 1H, *J*=7.2 Hz), 5.57 (t, 1H, *J*=5.6 Hz), 6.74 (d, 2H, *J*=8.0 Hz), 7.01 (d, 2H, *J*=7.6 Hz), 7.23–7.28 (m, 3H), 7.29–7.33 (m, 2H), 7.42–7.47 (m, 6H), 7.51–7.55 (m, 3H); ^{13}C NMR ($CDCl_3$, 100 MHz) δ 23.1, 44.2, 44.9, 123.1 (d, *J*=17.5 Hz), 127.4, 127.5, 127.6, 128.5 (d, *J*=11.6 Hz), 128.6, 130.6 (s), 130.7 (d, *J*=98.6 Hz) (s), 131.6 (d, *J*=2.6 Hz), 132.6 (d, *J*=9.7 Hz), 137.8 (s), 150.1 (s), 167.6 (s); ^{31}P NMR ($CDCl_3$, 121.4 MHz, H_3PO_4) δ 3.40; HRMS (ESI): *m*/*z*: calcd for $C_{34}H_{31}N_2OPS$: 546.1895; found: 546.1898.

3.7. Preparation of phosphazide 11

To a solution of the azide **9b** (1.49 g, 5 mmol) in anhydrous diethyl ether (30 mL) tris(dimethylamino)phosphine (0.82 g, 5 mmol) was added. The resulting mixture was stirred at room temperature in an atmosphere of nitrogen for 6 h. Then the precipitated solid was isolated by filtration.

3.7.1. Phosphazide ***11*** *(R^2=C_6H_5–CH_2; R^3=H; R=$N(CH_3)_2$)*

The ^{1}H and ^{13}C NMR spectra of compound **11** at room temperature (in $CDCl_3$) displayed doubling of the majority of signals, suggesting the presence of two rotamers in a ratio 1:2.1.

Yield 78%; mp 150–153 °C (colorless prisms); IR (Nujol) 3133, 1544, 1505, 1345, 1280, 1255, 1163, 1065, 992, 855, 841, 755, 731, 703, 658 cm^{-1}; ^{1}H NMR ($CDCl_3$, 300 MHz) δ 2.65 (d, 18H_{mayor}, *J*=9.2 Hz), 2.67 (d, 18H_{minor}, *J*=9.2 Hz), 4.34 (d, 2H_{minor}, *J*=5.6 Hz), 4.69 (d, 2H_{mayor}, *J*=5.2 Hz), 5.38 (s, 2H_{mayor}), 5.43 (s, 2H_{minor}), 6.92 (br s, 1H_{mayor}), 7.02 (br s, 1H_{minor}), 7.11–7.38 (m, 18H); ^{13}C NMR ($CDCl_3$, 75 MHz) δ 37.2, 47.1, 49.0, 72.2, 73.5, 120.6, 127.5, 127.6, 127.7, 128.5, 128.6, 128.8, 129.0, 131.6 (s), 132.0 (s), 136.4 (s), 136.8 (s), 152.1 (s), 152.5 (s), 189.5 (s), 190.3 (s); ^{31}P NMR ($CDCl_3$, 121.4 MHz, H_3PO_4) δ 42.45; HRMS (ESI): *m*/*z*: calcd for $C_{21}H_{32}N_7OPS$: 461.2127; found: 461.2131.

3.8. Preparation of phosphazene 10f

A solution of the phosphazide **11** (1 mmol) in anhydrous toluene was heated at 80 °C for 16 h. Then the solvent was removed under reduced pressure to give **10f** as viscous oil.

3.8.1. Phosphazene ***10f*** *(R^2=C_6H_5–CH_2; R^3=H; R=$N(CH_3)_2$)*

Yield 64%; oil; IR (Neat) 3205, 1667, 1602, 1507, 1454, 1352, 1293, 1265, 1193, 1065, 982, 840, 737, 701 cm^{-1}; ^{1}H NMR ($CDCl_3$, 400 MHz) δ 2.61 (d, 18H; *J*=9.6 Hz), 4.06 (s, 2H), 4.41 (d, 2H, *J*=5.2 Hz), 5.53 (t, 1H, *J*=5.2 Hz), 6.65 (d, 2H, *J*=8.0 Hz), 6.97 (d, 2H, *J*=8.0 Hz), 7.08–7.11 (m, 1H), 7.15–7.22 (m, 2H), 7.24–7.28 (m, 2H); ^{31}P NMR ($CDCl_3$, 121.4 MHz, H_3PO_4) δ 22.32; HRMS (ESI): *m*/*z*: calcd for $C_{21}H_{32}N_5OPS$: 433.2065; found: 433.2068.

3.9. Computational details

All structures were optimized using the functional B3LYP[36] and the 6-31+G** basis set[37] as implemented in the Gaussian 03 suite of programs.[38] All energy minima and transition structures were characterized by frequency analysis. The energies reported in this work include the zero-point vibrational energy corrections (ZPVE) and are not scaled. The intrinsic reaction coordinates (IRC)[39] were followed to verify the energy profiles connecting each transition state to the correct local minima, by using the second-order Gonzalez–Schlegel integration method.[40] Wiberg bond orders[41] and natural atomic charges were calculated within the natural bond orbital (NBO) analysis.[42] The asynchronicity[23,43] of the reactions was determined by using a previously described approach.[23] The solvent effects have been considered by B3LYP/6-31+G** calculations using a Self-Consistency Reaction Field (SCRF)[44] method, based on the Polarized Continuum Model (PCM)[45] of Tomasi and co-workers, in diethyl ether as solvent. The topological properties of the electron density at the bond critical points (BCPs) have been characterized with the AIMPAC package[46] in the framework of the quantum theory of atoms in molecules (QTAIM) developed by Bader.[25,47]

Acknowledgements

This work was supported by the MCYT and FEDER (Projects CTQ2005-02323/BQU and CTQ2008-05827/BQU), and Fundación

Séneca-CARM (Project 08661/PI/08). M.-M. Ortin thanks the Fundación Cajamurcia for a fellowship. Thanks are given to Prof. Ibon Alkorta for helpful comments.

Supplementary data

Supplementary data associated with this article can be found in the online version, at doi:10.1016/j.tet.2009.01.064.

References and notes

1. (a) Newman, M. S.; Karnes, H. A. *J. Org. Chem.* **1966**, *31*, 3980–3984; (b) Kwart, H.; Evans, E. R. *J. Org. Chem.* **1966**, *31*, 410–412; For a recent review see: (c) Lloyd-Jones, G. C.; Moseley, J. D.; Renny, J. S. *Synthesis* **2008**, 661–689.
2. (a) Relles, H. M.; Pizzolato, G. *J. Org. Chem.* **1968**, *33*, 2249–2253; (b) Miyazaki, K. *Tetrahedron Lett.* **1968**, *9*, 2793–2798; (c) For a computational study on the mechanism of the Newman–Kwart rearrangement see: Jacobsen, H.; Donahue, J. *Can. J. Chem.* **2006**, *84*, 1567–1574.
3. (a) Gilday, J. P.; Lenden, P.; Moseley, J. D.; Cox, B. G. *J. Org. Chem.* **2008**, *73*, 3130–3134; (b) Moseley, J. D.; Lenden, P. *Tetrahedron* **2007**, *63*, 4120–4125; (c) Moseley, J. D.; Lenden, P.; Thomson, A. D.; Gilday, J. P. *Tetrahedron Lett.* **2007**, *48*, 6084–6087; (d) Moseley, J. D.; Sankey, R. F.; Tang, O. N.; Gilday, J. P. *Tetrahedron* **2006**, *62*, 4685–4689.
4. Sakamoto, M.; Yoshiaki, M.; Takahashi, M.; Fujita, T.; Watanabe, S. *J. Chem. Soc., Perkin Trans. 1* **1995**, 373–375.
5. (a) Harano, K.; Kiyonaga, H.; Hisano, T. *Tetrahedron Lett.* **1991**, *32*, 7557–7558; (b) Hayashi, T. *Tetrahedron Lett.* **1990**, *31*, 4155–4158; (c) Ziegler, F. E.; Zheng, Z.-L. *Tetrahedron Lett.* **1987**, *28*, 5973–5976; (d) Gais, H.-J.; Böhme, A. *J. Org. Chem.* **2002**, *67*, 1153–1161; (e) Faulkner, D. J.; Petersen, M. R. *J. Am. Chem. Soc.* **1973**, *95*, 553–563.
6. Young, D. W.; Robinson, M. J. T. *Tetrahedron Lett.* **1987**, *28*, 3631–3632.
7. Molina, P.; Alajarín, M.; Fresneda, P. M.; Lidón, J.; Vilaplana, M. J. *Synthesis* **1982**, 598–599.
8. (a) Schönberg, A.; Vargha, J. *Chem. Ber.* **1930**, *63*, 178–180; (b) Freudengerg, K.; Wolf, A. *Chem. Ber.* **1927**, *60*, 232–238; (c) Nayak, U. G.; Whistler, R. L. *J. Org. Chem.* **1969**, *34*, 3819–3822; (d) Schönberg, A. *Justus Liebigs Ann. Chem.* **1930**, *483*, 107–114.
9. Villemin, D.; Hachemi, M. *Synth. Commun.* **1996**, *26*, 2449–2459.
10. Degani, I.; Fochi, R.; Regondi, V. *Synthesis* **1981**, 149–151.
11. (a) Diana, M. B.; Marchetti, M.; Melloni, G. *Tetrahedron: Asymmetry* **1995**, *6*, 1175–1179; (b) Harano, K.; Shinohara, I.; Murase, M.; Hisano, T. *Heterocycles* **1987**, *26*, 2583–2586; (c) Harano, K.; Kiyonaga, H.; Sugimoto, S.-I.; Matsuoka, T.; Hisano, T. *Heterocycles* **1988**, *27*, 2327–2330; (d) Harano, K.; Shinohara, I.; Sugimoto, S.-I.; Matsuoka, T.; Hisano, T. *Chem. Pharm. Bull.* **1989**, *37*, 576–581.
12. Cristol, S. J.; Seapy, D. G. *J. Org. Chem.* **1982**, *47*, 132–136.
13. (a) Alajarin, M.; Vidal, A.; Ortin, M.-M. *Tetrahedron Lett.* **2003**, *44*, 3027–3030; (b) Alajarin, M.; Vidal, A.; Ortin, M.-M. *Org. Biomol. Chem.* **2003**, *1*, 4282–4292; (c) Alajarin, M.; Vidal, A.; Ortin, M.-M.; Bautista, D. *New J. Chem.* **2004**, *28*, 570–577; (d) Alajarin, M.; Vidal, A.; Ortin, M.-M.; Bautista, D. *Synlett* **2004**, 991–994.
14. Staudinger, H.; Meyer, J. *Helv. Chim. Acta* **1919**, *2*, 635–646.
15. Only when 4-CH_3–$C_6H_4CH_2OC(S)NHPh$ was heated in toluene solution under vigorous conditions (sealed tube, 140 °C, 48 h) a 40% of conversion to the rearranged 4-CH_3–$C_6H_4CH_2SC(O)NHPh$ was observed.
16. Carl, P. L.; Chakravarty, P. K.; Katzenellenbogen, J. A. *J. Med. Chem.* **1981**, *24*, 479–480.
17. (a) Warnecke, A.; Kratz, F. *J. Org. Chem.* **2008**, *73*, 1546–1552; (b) Greenwald, R. B.; Pedri, A.; Conover, C. D.; Zhao, H.; Choe, Y. H.; Martinez, A.; Shum, K.; Guan, S. *J. Med. Chem.* **1999**, *42*, 3657–3667; (c) For a review, see: Wakselman, M. *Nouv. J. Chem.* **1983**, *7*, 439–447.
18. (a) Damen, E. W. P.; Nevalainen, T. J.; van der Berg, T. J. M.; de Groot, F. M. H.; Scheeren, H. W. *Bioorg. Med. Chem.* **2002**, *10*, 71–77; (b) Griffin, R. J.; Evers, E.; Davidson, R.; Gibson, A. E.; Layton, D.; Irwing, W. J. *J. Chem. Soc., Perkin Trans. 1* **1996**, 1205–1211.
19. van Brankel, R.; Vulders, R. C. M.; Bokdam, R. J.; Grüll, H.; Robillard, M. *Bioconjugate Chem.* **2008**, *19*, 714–718.
20. (a) Verkade, J. G.; Kisanga, P. B. *Tetrahedron* **2003**, *59*, 7819–7858 and references cited therein; (b) Liu, X.; Thirupathi, I. A.; Guzei, J. G.; Verkade, J. G. *Inorg. Chem.* **2004**, *43*, 7431–7440; (c) Venkat Reddy, Ch.; Verkade, J. G. *J. Org. Chem.* **2007**, *72*, 3093–3096.
21. Kukhar, V. P.; Patreshenko, A. A.; Zhumorova, I. N.; Tukhar, A. A.; Solodushenko, S. N. *Zh. Obshch. Khim.* **1970**, *40*, 1696–1699.
22. The planes shown in this figure have been calculated using the software Mercury 1.4.1. Macrae, C. F.; Edgington, P. R.; McCabe, P.; Pidcock, E.; Shields, G. P.; Taylor, R.; Towler, M.; de Streek, J. v. *J. Appl. Crystallogr.* **2006**, *39*, 453–457. See also: http://www.ccdc.cam.ac.uk/mercury/.
23. Moyano, A.; Pericas, M. A.; Valenti, E. *J. Org. Chem.* **1989**, *54*, 573–582.
24. (a) Queral, J. J.; Safont, V. S.; Moliner, V.; Andres, J. *Chem. Phys.* **1998**, *229*, 125–136; (b) Domingo, L. R.; Picher, M. T.; Safont, V. S.; Andres, J.; Chuchani, G. *J. Phys. Chem. A* **1999**, *103*, 3935–3943; (c) Rotinov, A.; Chuchani, G.; Andres, J.; Domingo, L. R.; Safont, V. S. *Chem. Phys.* **1999**, *246*, 1–12.
25. Bader, R. F. W. *Atoms in Molecules: A Quantum Theory*; Oxford University Press: Oxford, UK, 1990.
26. Jencks, W. P. *Chem. Soc. Rev.* **1981**, *10*, 345–375.
27. Domingo, L. R.; Saez, J. A.; Zaragoza, R. J.; Arnó, M. *J. Org. Chem.* **2008**, *73*, 4615–4624.
28. (a) Ross, J. A.; Seiders, R. P.; Lemal, D. M. *J. Am. Chem. Soc.* **1976**, *98*, 4325–4327; (b) Birney, D. M.; Wagenseller, P. E. *J. Am. Chem. Soc.* **1994**, *116*, 6262–6270; (c) Wagenseller, P. E.; Birney, D. M.; Roy, D. *J. Org. Chem.* **1995**, *60*, 2853–2859; (d) Birney, D. M. *J. Org. Chem.* **1996**, *61*, 243–251; (e) Birney, D. M.; Xu, X.; Ham, S. *Angew. Chem., Int. Ed.* **1999**, *38*, 189–193; (f) Fabian, W. M. F.; Kappe, C. O.; Bakulev, V. A. *J. Org. Chem.* **2000**, *65*, 47–53; (g) de Lera, A. R.; Alvarez, R.; Lecea, B.; Torrado, A.; Cossio, F. P. *Angew. Chem., Int. Ed.* **2001**, *40*, 557–561; (h) Birney, D. M. *Org. Lett.* **2004**, *6*, 851–854; (i) Cabaleiro-Lago, E. M.; Rodriguez-Otero, J.; Garcia-Lopez, R. M.; Peña-Gallego, A.; Hermida-Ramon, J. M. *Chem.—Eur. J.* **2005**, *11*, 5966–5974; (j) Jones, G. O.; Xuechen, L.; Hayden, A. E.; Houk, K. N.; Danishefsky, S. J. *Org. Lett.* **2008**, *10*, 4093–4096.
29. For our previous results on pseudopericyclic reactions see: (a) Alajarin, M.; Ortin, M.-M.; Sanchez-Andrada, P.; Vidal, A. *J. Org. Chem.* **2006**, *71*, 8126–8139; (b) Alajarin, M.; Ortin, M.-M.; Sanchez-Andrada, P.; Vidal, A.; Bautista, D. *Org. Lett.* **2005**, *7*, 5281–5284; (c) Alajarin, M.; Sanchez-Andrada, P.; Vidal, A.; Tovar, F. *J. Org. Chem.* **2005**, *70*, 1340–1349; (d) Lisowskaya, N. A.; Alajarin, M.; Sanchez-Andrada, P. *Eur. J. Org. Chem.* **2005**, 1468–1475; (e) Alajarin, M.; Sanchez-Andrada, P.; Cossio, F. P.; Arrieta, A.; Lecea, B. *J. Org. Chem.* **2001**, *66*, 8470–8477; (f) Alajarin, M.; Vidal, A.; Sanchez-Andrada, P.; Tovar, F.; Ochoa, G. *Org. Lett.* **2000**, *2*, 965–968.
30. Silva, C.; Nieto, O.; Souto, J. A.; Alvarez, R.; de Lera, A. *J. Comput. Chem.* **2007**, *28*, 1411–1416.
31. Tsuji, Y.; Richard, J. P. *J. Am. Chem. Soc.* **2006**, *128*, 17138–17145.
32. Smolinsky, G. J. *J. Org. Chem.* **1961**, *26*, 4108–4110.
33. Cuevas, J. C.; Mendoza, J.; Prados, P. *J. Org. Chem.* **1988**, *53*, 2055–2066.
34. Alajarin, M.; Lopez-Lazaro, A.; Vidal, A.; Berna, J. *Chem.—Eur. J.* **1998**, *4*, 2558–2570.
35. Merrill, S. H.; Unruh, C. C. U.S. Patent 3,002,003, 1959; *Chem. Abstr.* **1962**, *56*, 4961i.
36. (a) Parr, R. G.; Yang, W. *Density-Functional Theory of Atoms and Molecules*; Oxford University Press: New York, NY, 1989; (b) Bartolotti, L. J.; Fluchichk, K. In *Reviews in Computational Chemistry*; Lipkowitz, K. B., Boyds, D. B., Eds.; VCH: New York, NY, 1996; Vol. 7, pp 187–216; (c) Kohn, W.; Becke, A. D.; Parr, R. G. *J. Phys. Chem.* **1996**, *100*, 12974–12980; (d) Ziegler, T. *Chem. Rev.* **1991**, *91*, 651–667.
37. Hariharan, P. C.; Pople, J. *Theor. Chim. Acta* **1973**, *28*, 213–222.
38. Frisch, M. J.; Trucks, G. W.; Schlegel, H. B.; Scuseria, G. E.; Robb, M. A.; Cheeseman, J. R.; Montgomery, J. A., Jr.; Vreven, T.; Kudin, K. N.; Burant, J. C.; Millam, J. M.; Iyengar, S. S.; Tomasi, J.; Barone, V.; Mennucci, B.; Cossi, M.; Scalmani, G.; Rega, N.; Petersson, G. A.; Nakatsuji, H.; Hada, M.; Ehara, M.; Toyota, K.; Fukuda, R.; Hasegawa, J.; Ishida, M.; Nakajima, T.; Honda, Y.; Kitao, O.; Nakai, H.; Klene, M.; Li, X.; Knox, J. E.; Hratchian, H. P.; Cross, J. B.; Adamo, C.; Jaramillo, J.; Gomperts, R.; Stratmann, R. E.; Yazyev, O.; Austin, A. J.; Cammi, R.; Pomelli, C.; Ochterski, J. W.; Ayala, P. Y.; Morokuma, K.; Voth, G. A.; Salvador, P.; Dannenberg, J. J.; Zakrzewski, V. G.; Dapprich, S.; Daniels, A. D.; Strain, M. C.; Farkas, O.; Malick, D. K.; Rabuck, A. D.; Raghavachari, K.; Foresman, J. B.; Ortiz, J. V.; Cui, Q.; Baboul, A. G.; Clifford, S.; Cioslowski, J.; Stefanov, B. B.; Liu, G.; Liashenko, A.; Piskorz, P.; Komaromi, I.; Martin, R. L.; Fox, D. J.; Keith, T.; Al-Laham, M. A.; Peng, C. Y.; Nanayakkara, A.; Challacombe, M.; Gill, P. M. W.; Johnson, B.; Chen, W.; Wong, M. W.; Gonzalez, C.; Pople, J. A. *Gaussian 03* Revision B.03; Gaussian: Pittsburgh, PA, 2003.
39. (a) Fukui, K. *J. Phys. Chem.* **1970**, *74*, 4161–4162; (b) Fukui, K. *Acc. Chem. Res.* **1981**, *14*, 363–368.
40. (a) Gonzalez, C.; Schlegel, H. B. *J. Phys. Chem.* **1990**, *94*, 5523–5527; (b) Gonzalez, C.; Schlegel, H. B. *J. Chem. Phys.* **1991**, *95*, 5853–5860.
41. Wiberg, K. B. *Tetrahedron* **1968**, *24*, 1083–1096.
42. (a) Reed, A. E.; Weinstock, R. B.; Weinhold, F. *J. Chem. Phys.* **1985**, *83*, 735–746; (b) Reed, A. E.; Curtiss, L. A.; Weinhold, F. *Chem. Rev.* **1988**, *88*, 899–926; (c) Reed, A. E.; Schleyer, P. v. R. *J. Am. Chem. Soc.* **1990**, *112*, 1434–1445.
43. Borden, W. T.; Loncharich, R. J.; Houk, K. N. *Annu. Rev. Phys. Chem.* **1988**, *39*, 213–236.
44. (a) Tomasi, J.; Persico, M. *Chem. Rev.* **1994**, *94*, 2027–2094; (b) Simkin, B. Y.; Sheikhet, I. *Quantum Chemical and Statistical Theory of Solutions: A Computational Approach*; Ellis Horwood: London, UK, 1995, pp 78–101.
45. (a) Miertus, S.; Scrocco, E.; Tomasi, J. *J. Chem. Phys.* **1981**, *55*, 117–129; (b) Cammi, R.; Tomasi, J. *J. Chem. Phys.* **1994**, *100*, 7495–7502; (c) Barone, V.; Cossi, M.; Tomasi, J. *J. Chem. Phys.* **1997**, *107*, 3210–3221.
46. Biegler-Koenig, F. W.; Bader, R. F. W.; Tang, T. H. *J. Comput. Chem.* **1982**, *3*, 317–328 The AIMPAC package is available at: http://www.chemistry.mcmaster.ca/aimpac.
47. (a) A recent survey of QTAIM theory is due to Popelier P. L. A.; Aicken F. M.; O'Brien S. E. Chemical Modelling: Applications and Theory; The Royal Society of Chemistry: Cambridge, UK, 2000;Vol. 1, pp 143–198. See also: (b) Popelier, P. *Atoms in Molecules: An Introduction*; Prentice Hall: New York, NY, 2000; (c) Merino, G.; Vela, A.; Heine, T. *Chem. Rev.* **2006**, *105*, 3812–3841; (d) *The Quantum Theory of Atoms in Molecules: From Solid State to DNA and Drug Design*; Matta, C. F., Boyd, R. J., Eds.; Wiley-VCH: Weinheim, 2007.